Trisomy 21 consistently activates the interferon response

Kelly D. Sullivan[1,2,3,4]*, Hannah C. Lewis[1,2], Amanda A. Hill[1,2], Ahwan Pandey[1,2,3,4], Leisa P. Jackson[1,3,4], Joseph M. Cabral[1,3,4], Keith P. Smith[1], L. Alexander Liggett[1,5], Eliana B. Gomez[1,3,4], Matthew D. Galbraith[1,2,3,4], James DeGregori[1,5,6], and Joaquín M. Espinosa[1,2,3,4]*

[1]Linda Crnic Institute for Down Syndrome, University of Colorado School of Medicine, Aurora, Colorado 80045, USA

[2]Department of Pharmacology, University of Colorado School of Medicine, Aurora, Colorado 80045, USA

[3]Department of Molecular, Cellular and Developmental Biology, University of Colorado Boulder, Boulder, Colorado 80203, USA

[4]Howard Hughes Medical Institute, Chevy Chase, Maryland 20815, USA

[5]Department of Biochemistry and Molecular Genetics, University of Colorado School of Medicine, Aurora, Colorado 80045, USA

[6]Department of Pediatrics, Integrated Department of Immunology, Section of Hematology, Department of Medicine, University of Colorado School of Medicine, Aurora, CO 80045.

*Correspondence to: joaquin.espinosa@ucdenver.edu / kelly.d.sullivan@ucdenver.edu

ABSTRACT

Although it is clear that trisomy 21 causes Down syndrome, the molecular events acting downstream of the trisomy remain ill defined. Using complementary genomics analyses, we identified the interferon pathway as the major signaling cascade consistently activated by trisomy 21 in human cells. Transcriptome analysis revealed that trisomy 21 activates the interferon transcriptional response in fibroblast and lymphoblastoid cell lines, as well as circulating monocytes and T cells. Trisomy 21 cells show increased induction of interferon-stimulated genes and decreased expression of ribosomal proteins and translation factors. An shRNA screen determined that the interferon-activated kinases JAK1 and TYK2 suppress proliferation of trisomy 21 fibroblasts, and this defect is rescued by pharmacological JAK inhibition. Therefore, we propose that interferon activation, likely via increased gene dosage of the four interferon receptors encoded on chromosome 21, contributes to many of the clinical impacts of trisomy 21, and that interferon antagonists could have therapeutic benefits.

INTRODUCTION

Trisomy 21 (T21) is the most common chromosomal abnormality in the human population, occurring in approximately 1 in 700 live births (Alexander et al. 2016). The extra copy of chromosome 21 (chr21) impacts human development in diverse ways across every major organ system, causing the condition known as Down syndrome (DS). One of the most intriguing aspects of T21 is that it causes an altered disease spectrum in the population with DS, protecting these individuals from some diseases (e.g. solid tumors, hypertension), while strongly predisposing them to others (e.g. Alzheimer's disease, leukemia, autoimmune disorders) (Alexander et al. 2016; Sobey et al. 2015; Bratman et al. 2014; Roberts and Izraeli 2014; Anwar, Walker, and Frier 1998; Malinge et al. 2013; Hasle et al. 2016). Despite many years of study, the molecular, cellular, and physiological mechanisms driving both the protective and deleterious effects of T21 are poorly understood. A few chr21-encoded genes have been implicated in the development of specific comorbidities, such as *APP* in Alzheimer's disease (Wiseman et al. 2015), and *DYRK1A* and *ERG* in hematopoietic malignancies (Stankiewicz and Crispino 2013; Malinge et al. 2012). Therefore, research in this area could inform a wide range of medical conditions affecting not only those with DS, but also the typical population.

The clinical manifestation of DS is highly variable among affected individuals, with various comorbidities appearing in a seemingly random fashion, suggesting the presence of strong modifiers, genetic or otherwise, of the deleterious effects of T21. Even conserved features, such as cognitive impairment, display wide quantitative variation (de Sola et al. 2015). Collectively, our understanding of the mechanisms driving such inter-individual variation in the population with DS is minimal. More specifically, it is unclear what gene expression changes are consistently caused by T21, versus those that are context-dependent. Integrated analyses of a large body of studies have indicated that the changes in gene expression caused by T21 involve various signaling pathways (Scarpato et al. 2014), however, these studies vary widely in cell type, number of samples, and even analysis platform, among other variables (Volk et al. 2013;

63 Costa et al. 2011). More recently, gene expression analysis of cells derived from discordant
64 monozygotic twins, only one of which was affected by T21, concluded that global gene
65 expression changes in T21 cells are driven by differences in chromatin topology, whereby
66 affected genes are clustered into large chromosomal domains of activation or repression
67 (Letourneau et al. 2014). However, independent re-analysis of these data has challenged this
68 conclusion (Do, Mobley, and Singhal 2015). Therefore, there remains a clear need to identify
69 the consistent gene expression changes caused by T21 and to characterize how these
70 programs are modified across cell types, tissue types, genetic backgrounds, and developmental
71 stages.

72 In order to identify *consistent* signaling pathways modulated by T21, defined as those
73 that withstand the effects of inter-individual variation, we employed two complementary
74 genomics approaches, transcriptome analysis and shRNA loss-of-function screening, in both
75 panels of cell lines and primary cell types from individuals of diverse genetic background,
76 gender, and age, with and without T21. Our RNA-seq transcriptome analysis identified
77 *consistent* gene expression signatures associated with T21 in all cell types examined.
78 Interestingly, the fraction of this gene expression signature that is not encoded on chr21 is
79 dominated by the interferon (IFN) transcriptional response, an observation that is reproducible in
80 skin fibroblasts, B cell-derived lymphoblastoid cell lines, as well as primary monocytes and T
81 cells. In parallel, we performed a kinome-focused shRNA screen that identified the IFN-
82 activated kinases JAK1 and TYK2 as strong negative regulators of T21 cell proliferation in
83 fibroblasts. Importantly, pharmacological inhibition of JAK kinases improves T21 cell viability.
84 Taken together, our results identify the IFN pathway as a *consistent* signaling pathway activated
85 by T21, which could merely be a result of increased gene dosage of four IFN receptor subunits
86 encoded on chr21. We hypothesize that IFN activation could contribute to many of the effects of
87 T21, including increased risk of leukemia and autoimmune disorders, as well as many

88 developmental abnormalities also observed in interferonopathies (Yao et al. 2010; Zitvogel et al.
89 2015; Crow and Manel 2015; McGlasson et al. 2015).
90
91 **RESULTS**
92 **Trisomy 21 causes consistent genome-wide changes in gene expression.**
93 In order to investigate *consistent* gene expression signatures associated with T21, we
94 performed RNA-seq on a panel of 12 age- and gender-matched human fibroblasts from euploid
95 (disomic, D21) and T21 individuals (Figure 1 – figure supplement 1A-C). T21 was confirmed by
96 PCR analysis of the chr21-encoded *RCAN1* gene (Figure 1 – figure supplement 1D). We
97 included samples from different genetic backgrounds, ages, and genders, in order to avoid
98 identifying differences that are specific to a particular pair of isogenic or genetically related cell
99 lines and which would not withstand the effects of inter-individual variation. To illustrate this
100 point, comparison of one pair of disomic male individuals of similar age yielded thousands of
101 differentially expressed genes (DEGs), with similar numbers of upregulated and downregulated
102 DEGs (Figure 1A-B, Male 1 vs. Male 2). However, when the 12 samples are divided into two
103 groups with roughly balanced age, gender, and T21 status, very few consistent changes were
104 identified, thus demonstrating the impact of inter-individual variation within our sample set
105 (Figure 1A-B, Figure 1 –figure supplement 1C, Group 1 vs. Group 2). In contrast, comparison of
106 all T21 versus all D21 cells identified 662 consistent DEGs, with a disproportionate number of
107 these upregulated in T21 cells (471 of 662, Figure 1A, T21 vs. D21, Supplementary file 1A). We
108 also observed an uncharacteristic spike of DEGs at ~1.5-fold overexpression in T21 cells on a
109 volcano plot, consistent with many chr21 genes being overexpressed solely due to increased
110 gene dosage (Figure 1B). For comparison purposes, we also analyzed samples by gender
111 which expectedly yielded DEGs encoded on chrX (e.g. *XIST*) and chrY (Figure 1 A-B; Female
112 vs. Male). Gender causes fewer significant changes than T21, with roughly equal numbers of
113 upregulated and downregulated genes. Taken together, these data indicate that T21 produces

114 consistent changes in a gene expression signature that withstands differences in genetic
115 background, age, gender, and site of biopsy. Of note, when we performed RNA-seq analysis
116 using increasing numbers of T21 vs. D21 pairs, the fraction of chr21-encoded DEGs increased
117 steadily with sample size, accounting for ~12% of the core gene expression signature in the 12
118 cell line panel. However, 88% of DEGs are located on other chromosomes, indicating the
119 existence of conserved mechanisms driving these genome-wide changes in gene expression
120 (Figure 1 – figure supplement 1E).

121 A recent report concluded that changes in gene expression caused by T21 between a
122 single pair of discordant monozygotic twins were due to dysregulation of chromosomal domains
123 (Letourneau et al. 2014). Thus, we next asked where the ~88% of core DEGs not encoded on
124 chr21 are located across the genome. This exercise revealed broad distribution across all
125 chromosomes, with no obvious contiguous domains of up- or downregulation (see Figure 1 –
126 figure supplement 2A for a whole genome Manhattan plot, and Figure 1 – figure supplement 3
127 for individual chromosomes). In fact, mere visual analysis of DEGs from the individual
128 chromosomes previously claimed by Letourneau et al. to harbor large dysregulated domains
129 (e.g. chr3, chr11, chr19) did not reveal such domains in our dataset, showing instead obvious
130 regions of overlapping activation and repression (shaded gray boxes in Figure 1C). Thus, our
131 analysis is more consistent with the report that re-analyzed the data in Letournaeu et al. and
132 questioned the existence of these chromosomal domains (Do, Mobley, and Singhal 2015). In
133 fact, the only region of the genome at which there was clear contiguous upregulation of DEGs
134 was chr21 itself (Figure 1C, Figure 1 – figure supplements 2A and 3).

135 In order to characterize the mechanism driving the consistent changes caused by T21,
136 we examined the regulatory differences between DEGs encoded on chr21 and those not
137 encoded on chr21. Several lines of evidence indicate that, while chr21 DEGs are regulated
138 mostly by increased gene dosage, non-chr21 DEGs may be driven by specific pathways that
139 are subject to signal amplification, with a bias toward upregulation, and greatly affected by inter-

140 individual variation. First, violin plots display the relatively small number of chr21 DEGs,
141 showing mostly upregulation clustered around 1.5 fold, versus a much larger number of non-
142 chr21 DEGs, showing both up- and downregulation with no obvious clustering of fold changes
143 (Figure 1D, Figure 1 – figure supplement 2B). Second, the obvious effect of gene dosage on the
144 expression of chr21 DEGs is apparent in the violin plots and heatmaps (Figure 1D, E), where
145 the median fold change centers around 1.5 fold (e.g. *APP*, *ETS2*), while a few genes show
146 greater induction (e.g. *MX1*, *MX2*). In fact, chr21 genes exhibit more than an 80% probability of
147 a ~1.5-fold change as calculated by kernel density estimation analysis (Figure 1F). Third, the
148 bias toward upregulation among non-chr21 DEGs is evident in the violin plots, heatmaps, and
149 density estimation analysis (Figure 1D-F), where a larger fraction of these genes are
150 upregulated. Finally, we measured the inter-individual variation of chr21 DEGs versus non-
151 chr21 DEGs by calculating the standard deviation for each DEG across each age- and gender-
152 matched pair of fibroblasts. As shown in Figure 1G, the median standard deviation for chr21
153 DEGs is much smaller than for all DEGs.
154 Altogether, these results suggest the existence of consistent signaling pathways
155 activated by increased dosage of chr21 genes, which in turn cause global changes in gene
156 expression, with a bias toward upregulation and displaying strong inter-individual variation.
157
158 **Trisomy 21 leads to constitutive activation of the interferon transcriptional response.**
159 Next, we subjected T21 DEGs to upstream regulator analysis using Ingenuity Pathway
160 Analysis (IPA) to identify putative factors contributing to consistent changes in gene expression.
161 This analysis tool includes both a hypergeometric test for overlapping sets of genes and a
162 directional component to predict activation or inactivation of factors that control gene expression
163 (e.g. transcription factors, protein kinases) (Krämer et al. 2014). We confirmed the effectiveness
164 of this tool using published RNA expression datasets from our lab for cells treated with an
165 inhibitor of the p53-MDM2 interaction, hypoxia, and serum stimulation (Sullivan et al. 2012;

166 Donner et al. 2010; Galbraith et al. 2013). IPA effectively identified p53, the Hypoxia Inducible
167 Factor 1A (HIF1A), and growth factor receptors and downstream kinases (PDGF, ERK) as the
168 top upstream regulators in each scenario, respectively (Figure 2 – figure supplement 1A).
169 Strikingly, the top 13 upstream regulators predicted to be activated in T21 cells are all IFN-
170 related factors, including IFN ligands (e.g. IFNA2, IFNB, IFNG) and IFN-activated transcription
171 factors (e.g. IRF3, IRF5, IRF7, STAT1) (Figure 2A). Importantly, most of these signals are
172 derived from non-chr21 DEGs, and would be missed by analyses focused specifically on chr21-
173 encoded genes (Figure 2A). This analysis also identified two known repressors of IFN signaling,
174 MAPK1 and TRIM24, as upstream regulators inactivated in T21 cells, consistent with activation
175 of the IFN pathway (Huang et al. 2008; Tisserand et al. 2011). As an example of how the RNA-
176 seq data supports the upstream regulator prediction by IPA, Figure 2B shows the gene network
177 centered on the ligand IFNA2 as a potential driver of consistent gene expression changes.
178 Strong activation of the IFN pathway was also predicted using a different tool, the Pathway
179 Commons Analysis in WebGestalt (Zhang, Kirov, and Snoddy 2005; J. Wang et al. 2013;
180 Cerami et al. 2011), where 4 of the top 15 pathways identified were IFN-related (Figure 2 –
181 figure supplement 1B).
182 Notably, activation of IFN signaling in T21 cells could be explained by the fact that four
183 of the six IFN receptors, *IFNAR1*, *IFNAR2*, *IFNGR2*, and *IL10RB*, (representing each IFN class,
184 Type-I, -II, and -III), are chr21-encoded DEGs (Figure 2C, D). Using a combination of IPA
185 upstream regulator predictions and our RNA-seq data, we clearly identified the canonical IFN
186 pathways –from ligands through receptors and kinases and down to transcription factors and
187 IFN-stimulated genes (ISGs)– as activated in T21 cells (Figure 2C). Whereas IFN receptors are
188 upregulated ~1.5 fold with relatively low levels of inter-individual variation, as expected for
189 increased gene dosage in T21 cells, the downstream ISGs exhibit larger fold changes, greater
190 variation between samples, and tend to have low expression levels in D21 cells, in accord with
191 activation of IFN only of T21 cells (Figure 2D). We confirmed the elevated basal expression of

192 three of the IFN receptors (IFNAR1, IFNGR2, and ILR10RB), enhanced basal phosphorylation
193 of STAT1, as well as increased basal expression of several ISGs at the protein level in T21
194 cells, with noticeable inter-individual variation (Shuai et al. 1994; Waddell et al. 2010; Schoggins
195 et al. 2011) (Figure 2E).
196 We next analyzed protein lysates from the 12 fibroblast lines using SOMAScan
197 technology, which employs DNA aptamers to monitor epitope abundance (Gold et al. 2012;
198 Mehan et al. 2014; Hathout et al. 2015). This assay confirmed elevated protein levels for many
199 of the IFN-related genes found to be induced at the mRNA level in the RNA-seq experiment
200 (Figure 2F). Finally, we examined the fraction of our upregulated DEGs linked to IFN signaling
201 using IPA, Pathway Commons, and a list of 387 validated ISGs curated by Schoggins and
202 colleagues (Schoggins et al. 2011). Our analysis revealed that 21% (101/471) of DEGs
203 upregulated in T21 cells are linked to IFN signaling, with contributions from both chr21 (17%,
204 14/81) and non-chr21 (22%, 87/390) DEGs, pointing to IFN activation as a potential mechanism
205 for the larger number of upregulated versus downregulated DEGs (Figure 2 - figure supplement
206 1C). Altogether, these results indicate that the IFN pathway is consistently induced by trisomy
207 21 in fibroblasts, and that the IFN transcriptional response accounts for a considerable fraction
208 of the transcriptome changes caused by trisomy 21 across the genome.
209
210 **Trisomy 21 cells display stronger induction of ISGs upon stimulation with IFN ligands**
211 **than euploid cells.**
212 We next investigated whether T21 cells produce a stronger response to specific IFN
213 ligands than their D21 counterparts. To test this, we treated three pairs of fibroblasts –roughly
214 matched by age and gender– with various doses of the Type I ligands IFNα or β, or with the
215 Type II ligand IFNγ, and monitored expression of key ISGs via western blot. We also monitored
216 phosphorylation of STAT1. Overall, these efforts revealed that trisomy 21 cells show stronger

217 induction of ISGs upon treatment with all three ligands, albeit with variation across specific cell
218 lines and ligands (Figure 3). For example, stimulation with IFNα led to stronger induction in the
219 T21 cell line for MX1 in pairs 1 and 2, stronger induction of IDO1 in pairs 1 and 3, and stronger
220 induction of ISG15 in pairs 1 and 2 (Figure 3A). Similar results were observed for the other Type
221 I ligand, IFNβ. However, ligand-specific differences were also observed. For example, IDO1 was
222 more strongly induced by IFNα and β in the T21 cell line in pair 1, but this was not the case
223 when using IFNγ (Figure 3A-C). Thus, these results confirm the notion of strong inter-individual
224 variation in the downstream signaling effects of T21. Of note, all three IFN ligands consistently
225 induced STAT1 phosphorylation (pSTAT1) both in D21 and T21 cells, but the levels of pSTAT1
226 did not correlate precisely with the expression levels of the various ISGs. For example, the
227 obviously different levels of ISG15 in pair 2 upon treatment with the three ligands do not
228 correlate with dissimilar levels of pSTAT1 (Figure 3A-C). This suggests that STAT1
229 phosphorylation is not a robust predictor of ISG expression, which is ultimately defined by the
230 orchestrated action of multiple IFN-activated transcription factors.
231
232 **A kinome shRNA screen identifies the IFN-activated kinases JAK1 and TYK2 as negative**
233 **regulators of cell viability in trisomy 21 fibroblasts.**
234 In a parallel unbiased approach to identify signaling cascades deregulated by T21, we
235 employed an shRNA screen to identify protein kinases that may have a differential impact on
236 the viability (i.e. proliferation and/or survival) of T21 cells relative to D21 cells. We hypothesized
237 that core gene expression changes in T21 cells lead to a rewiring of signaling cascades,
238 creating differential requirements for specific kinases during cell survival and proliferation. In
239 order to identify such kinases, we introduced a library of 3,075 shRNAs targeting 654 kinases
240 into each of the 12 fibroblast cell lines we subjected to transcriptome analysis. We then
241 propagated these cells for 14 days to allow for selection of cells harboring shRNAs targeting

242 kinases that differentially affect survival and/or proliferation of T21 cells versus D21 cells,
243 henceforth referred to as DM^{T21} kinases (***D***ifferential ***M***odulators of ***T21*** cells) (Figure 4A). In this
244 screen, relative enrichment of a given shRNA in the T21 population could result from the
245 targeted kinase being a negative regulator of T21 cellular fitness, a positive regulator of D21
246 cellular fitness, or a combination of both. To minimize the possibility of shRNA off-target effects,
247 we required at least three independent shRNAs targeting a given kinase to score as significantly
248 enriched or depleted, with no more than one shRNA against each kinase scoring in the opposite
249 direction (see Materials and Methods for details). This analysis identified a total of 25 and 15
250 kinases that negatively and positively affect the fitness of T21 cells relative to D21 cells,
251 respectively (Figure 4B, Figure 4 – figure supplement 1, Supplementary file 2). The top scoring
252 enriched kinase was mTOR, indicating that this kinase differentially decreases the fitness of T21
253 cells (and/or differentially increases the fitness of D21 cells). This could be consistent with
254 previous reports showing hyperactivation of mTOR signaling in the brains of individuals with DS
255 and mouse models of trisomy 21 and consequent impairments in autophagy (Ahmed et al.
256 2013; Perluigi, Di Domenico, and Butterfield 2015; Troca-Marín et al. 2014; Iyer et al. 2014).
257 Importantly, among DM^{T21} kinases predicted to hinder T21 cell viability were the IFN-activated
258 kinases JAK1 and TYK2 (Müller et al. 1993; Stahl et al. 1994) (Figure 4B, C, Figure 4 - figure
259 supplement 1A, B). To confirm that JAK1 signaling negatively affects the relative viability of T21
260 cells, we treated two pairs of D21/T21 fibroblasts with increasing doses of the JAK1/2 inhibitor
261 ruxolitinib (Rux) (Tefferi, Litzow, and Pardanani 2011). Rux treatment led to decreased levels of
262 pSTAT1, decreased protein expression of MX1 –an ISG encoded on chr21–, and decreased
263 mRNA expression of several ISGs found to be upregulated in T21 fibroblasts in our RNA-seq
264 experiment (Figure 4D and Figure 4 –figure supplement 1C, D). To assess the impact of Rux
265 treatment on cell viability, we seeded equal numbers of D21 and T21 fibroblasts in the absence
266 or presence of increasing doses of the inhibitor, and counted the number of viable cells 3 days
267 post-seeding. Notably, the number of viable T21 cells was much lower in all conditions tested

268 (Figure 4E and Figure 4 – figure supplement 1E). However, whereas Rux treatment led to a
269 dose-dependent increase in the number of viable T21 cells, it also produced a decrease in the
270 number of viable D21 cells at the highest concentration. When the cell counts are represented
271 as T21/D21 ratios, it is clear that JAK inhibition has a differential effect on cell proliferation
272 between T21 and D21 cells (Figure 4F, G and Figure 4 – figure supplement 1F, G). This is
273 consistent with shRNAs targeting JAK1 (and TYK2) being differentially enriched in T21 cells
274 during the 14-day course of the screen. Ultimately, these data support the notion of differential
275 signaling requirements in T21 relative to D21 cells and identify two IFN-related kinases as
276 negative regulators of T21 fibroblast viability.
277
278 **Activation of the IFN response by trisomy 21 is conserved in lymphoblastoid cells.**
279 To test whether consistent changes in gene expression programs elicited by trisomy 21
280 are conserved across cell types, we performed RNA-seq on a panel of six age-matched, female
281 lymphoblastoid cell lines from D21 and T21 individuals (Figure 5 – figure supplement 1A-B).
282 These cell lines were generated by immortalizing B cells with Epstein Bar virus (EBV), thus
283 enabling us to compare a cell type of lymphocytic origin with the fibroblasts of mesenchymal
284 origin. Analysis of DEGs associated with T21 identified 1,538 genes both up and downregulated
285 with more upregulated DEGs (861 out of 1,538), as was seen in the fibroblasts (Figure 5A,
286 Supplementary file 1B). Similarly, a peak of highly significant DEGs with ~1.5-fold change,
287 comprised of chr21-encoded genes, is observed in a volcano plot (Figure 5B). Furthermore,
288 most DEGs are distributed across the genome, and not arranged into obvious chromosomal
289 domains (Figure 5C and Figure 5 – figure supplement 2). IPA revealed that the top upstream
290 regulators of the consistent gene expression signature driven by T21 in lymphoblastoids are
291 also IFN-related, and that this prediction is powered by non-chr21 DEGs (Figure 5D).
292 Comparison of DEGs from fibroblasts and lymphoblastoids demonstrates that many of the same
293 upstream regulators are predicted to be activated and are IFN-related factors (Figure 5E). All

294 four chr21-encoded IFN receptors are significantly upregulated in lymphoblastoids (Figure 5F),
295 as they are in fibroblasts. In fact, the most significant DEG encoded on chr21 is *IFNAR1* (Figure
296 5B). Increased basal protein expression was confirmed by western blot for IFNAR1 and IL10RB,
297 as well as for the interferon-related genes TBX21, GBP5 and BCL2L11 (BIM) (Figure 5G).
298 STAT1 phosphorylation was also elevated in the T21 lymphoblastoids (Figure 5G).
299 We next wanted to determine if the IFN signature was conserved in a mouse model of
300 Down syndrome. Dp16 mice were selected because they contain a region of mouse
301 chromosome 16 syntenic to human chromosome 21 that includes the IFN receptor cluster,
302 without triplication of non-syntenic regions (Z. Li et al. 2007). RNA-seq was performed on the
303 LSK (Lineage negative, Sca1 positive, c-Kit positive) population of multipotent hematopoietic
304 stem and progenitor cells obtained from the bone marrow of Dp16 mice and matched littermate
305 controls. These results confirmed that three of the four IFN receptors are upregulated in Dp16
306 mice (*Ifnar1*, *Ifnar2*, and *Ifngr2*), along with several canonical ISGs (Figure 5 – figure
307 supplement 3, Supplementary file 1C). Our results demonstrate that IFN activation by trisomy
308 21 is conserved in the hematopoietic lineage.
309
310 **The IFN response is activated in circulating blood cell types of individuals with trisomy**
311 **21.**
312 In order to determine whether our findings are applicable to living human individuals with
313 T21, we isolated monocytes, T cells, and B cells, from 10 individuals with T21 and seven D21
314 individuals. As for our cell line work, we included samples from both genders with varying ages
315 and genetic backgrounds (Figure 6 – figure supplement 1A, B). Monocytes and T cells were
316 subjected to transcriptome analysis by RNA-seq, and B cells used for IFN receptor surface
317 expression analysis by flow cytometry. The transcriptome analyses identified hundreds of
318 consistent gene expression changes associated with T21 in both cell types, with the expected
319 ~1.5x fold increase in chr21 gene expression (Figure 6 – figure supplement 1C, D). The IFN

320 receptors encoded on chr21 are significantly upregulated in circulating blood cell types from
321 individuals with T21, with the sole exception of *IFNGR2* in T cells (Figure 6A, B, Supplementary
322 file 1D). Flow cytometry detected a minor increase in surface expression of IFNAR1, IFNGR2,
323 and IL10RB, in the B cell population, but not for IFNGR1, which is not encoded on chr21 (Figure
324 6 –figure supplement 2). Once again, upstream regulator analysis identified IFN ligands and
325 IFN-activated transcription factors as predicted drivers of gene induction in T21 monocytes and
326 T cells (Figure 6C and Figure 6 – figure supplement 3) with many canonical ISGs scoring
327 among the most significantly induced genes (Figure 6A, B).
328 A comparison of the upstream regulator analyses for the four cell types included in this
329 study revealed both conserved and cell type-specific features. The upstream regulator analysis
330 shows that IFN activation is conserved, as is predicted inactivation of the IFN repressors
331 MAPK1 and TRIM24 (Figure 6C). However, a unique feature of the primary cell types -
332 monocytes and T cells- is a predicted inactivation of the gene expression program driven by the
333 transcription factor MYCN (Figure 6C). Comparison of the canonical pathways deregulated in all
334 four cell types confirms that IFN signaling is the top activated pathway, but also reveals that
335 monocytes and T cells, and to a lesser degree lymphoblastoids, show strong repression of the
336 EIF2 pathway (Figure 6D). Since both MYCN and EIF2 are potent regulators of protein
337 synthesis, we decided to investigate this observation in more detail.
338
339 **Trisomy 21 downregulates the translation machinery in primary monocytes and T cells.**
340 A well-established aspect of the IFN response is the selective control of protein
341 translation, purportedly to prevent the synthesis of viral proteins during the course of infection
342 (Johnson, Lerner, and Lancz 1968). Mechanistically, it has been shown that IFN signaling
343 impairs processing of rRNAs and controls the activity and/or expression of specific translation
344 factors (Walsh, Mathews, and Mohr 2013; Maroun 1978). On the other hand, the MYC family of
345 transcription factors are known drivers of ribosome biogenesis, protein synthesis and cell growth

346 (van Riggelen, Yetil, and Felsher 2010; Boon et al. 2001; S. Kim et al. 2000; Arabi et al. 2005).
347 Similarly, the EIF2 pathway is a key driver of protein translation, with eIF2 itself being an
348 essential translation initiation factor (Hinnebusch 2014). Analysis of the gene signatures
349 identified by IPA that predicted inactivation of both the MYCN transcriptional program and the
350 EIF2 pathway showed a substantial degree of overlap (Figure 7A, C, Supplementary file 1E). In
351 monocytes and T cells, the genes common between the two repressed programs encode
352 components of both the small and large ribosome subunits (i.e. RPS proteins in the 40S
353 complex and RPL proteins in the 60S complex) (Figure 7A, C, Figure 7 – figure supplements 1
354 and 2). Genes exclusive to the MYCN signature are enriched for metabolic enzymes and
355 translation elongation factors (EEFs). Genes exclusive to the EIF2 signature are enriched for
356 translation initiation factors (EIFs) and additional ribosomal proteins. Examples of RPSs, RPLs,
357 EEFs and EIFs downregulated in trisomy 21 cells are shown in Figure 7B and D (see also
358 Figure 7 – figure supplements 1 and 2). This result is consistent with reports that interferon
359 treatment results in global decreases in expression of the translational machinery in primary
360 PBMCs (Taylor et al. 2007; Gupta et al. 2012). Altogether, these results indicate that T21
361 causes a general downregulation of dozens of components of the protein synthesis machinery
362 in circulating monocytes and T cells.
363
364 **Trisomy 21 elicits cell type-specific IFN transcriptional responses.**
365 Having performed transcriptome analysis of cell types of different origins, we
366 investigated to what degree the gene expression changes caused by T21 are affected by cell
367 type-specific regulatory landscapes. A principal component analysis (PCA) shows the fibroblast
368 transcriptomes segregating strongly (PC1 80.5%) from those of the cell types of hematopoietic
369 origin (Figure 8A). B cell-derived lymphoblastoids and T lymphocytes cluster together, yet they
370 segregate away from the monocytes of myeloid origin (PC2, 11.3%). Within this background,
371 the global impact of the trisomy on the transcriptome is secondary to the effects of the cell type

372 of origin (Figure 8B). Next, we asked to what degree genes encoded on chr21 could be affected
373 by these cell type-specific regulatory landscapes. Indeed, it was easy to identify many chr21
374 genes displaying obvious differences in relative expression among cell types. For example, *APP*
375 is relatively more highly expressed in fibroblasts, *U2AF1* more highly expressed in
376 lymphoblastoids, *ETS2* more highly expressed in monocytes, and *DYRK1A* more highly
377 expressed in T cells (Figure 8C, Supplementary file 1F). The IFN receptors on chr21 also
378 showed some degree of cell type-specific expression (e.g. *IFNAR2* lowly expressed in
379 fibroblasts, *IFNGR2* lowly expressed in T cells, Figure 8D). Furthermore, relative differences in
380 cell type-specific expression is also evident for canonical ISGs (Figure 8E). These observations
381 led us to ask to what degree the IFN transcriptional response elicited by T21 is conserved
382 across cell types. To address this, we compared the DEGs comprising the T21-induced
383 *Interferon alpha* signature identified by IPA in each cell type (Figure 6C). Remarkably, this
384 exercise revealed a large degree of cell type-specificity, with most IFN-related genes being
385 differentially expressed in only one cell type (Figure 8F). In fact, the only common genes among
386 all four signatures are three IFNα-related genes encoded on chr21: *IFNAR1*, *IFNAR2*, and *MX1*.
387 Expectedly, lymphoblastoids and T cells showed a greater degree of overlap than other pairwise
388 comparisons. Overall, these results indicate that while T21 operates within, and is modulated
389 by, cell type-specific regulatory landscapes, it nonetheless activates the IFN transcriptional
390 response consistently by inducing different gene sets within this program. This is in stark
391 contrast to the notion that T21 affects gene expression either stochastically or through large
392 rearrangements of chromatin domains. In fact, Manhattan plots of the DEGs in monocytes and
393 T cells derived from the same individuals not only confirm the absence of large domains of
394 chromatin deregulation, but also highlight the high degree of cell type-specific changes caused
395 by the trisomy (Figure 8G).
396

397 **DISCUSSION.**

398 We report here that T21 leads to consistent activation of the IFN pathway. As discussed
399 below, IFN hyperactivation could explain many of the developmental and clinical impacts of T21.
400 In fact, we posit that Down syndrome can be understood largely as an interferonopathy, and
401 that the variable clinical manifestations of T21 could be explained by inter-individual differences
402 in adaptation to chronic IFN hyperactivity.

403 The link between IFN signaling and T21 is not entirely unprecedented. More than 40
404 years ago, it was found that human T21 fibroblasts, but not those trisomic for chr13 or chr18,
405 have increased sensitivity to IFN exposure and are more resistant to viral infection (Tan et al.
406 1974; Tan, Tischfield, and Ruddle 1974). In fact, somatic cell hybrid experiments showed that
407 chr21 is sufficient to confer sensitivity to human IFN in mouse cells (Slate et al. 1978).
408 Pioneering work by Maroun and colleagues using an early mouse model of DS carrying an extra
409 copy of chr16 that harbors orthologues of many human chr21 genes, including the four IFN
410 receptors, clearly implicated IFN as a contributor to the deleterious effects of the trisomy. For
411 example, treatment of pregnant female mice with anti-IFN antibodies resulted in partial rescue
412 of embryonic growth defects and embryonic lethality (Maroun 1995). Furthermore, partial
413 normalization of gene dosage for the IFN receptor subunits via gene knockout was shown to
414 improve embryonic development and survival of T21 cortical neurons *in vitro* (Maroun,
415 Heffernan, and Hallam 2000). More recently, a study found global disruption of IFN-related gene
416 networks in the brains of the Ts1Cje mouse model of DS, which also carries triplication of the
417 IFN receptor subunits (Ling et al. 2014). However, deeper investigations of IFN signaling in
418 human T21 cells and tissues are largely absent from the literature of the past 30 years, with a
419 few exceptions, such as the description of IFN signaling as a contributor to periodontal disease
420 in DS (Tanaka et al. 2012; Iwamoto et al. 2009). Collectively, these reports and the genomics
421 analyses reported here demonstrate that activation of the IFN pathway in T21 cells is a

422 widespread phenomenon that occurs in diverse tissues, and that is relevant to human Down
423 syndrome as well as the various mouse models of DS with triplication of IFN receptors.
424 Constitutive activation of IFN signaling could conceivably explain a large number of
425 comorbidities associated with DS, such as the increased risk of transient myeloproliferative
426 disorder, diverse leukemias, several autoimmune disorders (Richardson et al. 2010), and
427 perhaps even the lower rate of solid tumors (Zitvogel et al. 2015; Hasle et al. 2016). Importantly,
428 several JAK inhibitors are either approved or being tested in clinical trials for the treatment of
429 several conditions associated with DS –albeit in the typical population– , including
430 myeloproliferative, inflammatory and autoimmune disorders, as well as leukemia (Padron et al.
431 2016; Spaner et al. 2016; Tefferi, Litzow, and Pardanani 2011; Quintás-Cardama et al. 2010;
432 Shi et al. 2014; Keystone et al. 2015; Jabbari et al. 2015). It should be noted, however, that the
433 dose limiting toxicities of JAK inhibitors, like ruxolitinib, are anemia and thrombocytopenia
434 (McKeage 2015; Plosker 2015). Therefore, rigorous clinical investigations will be required to
435 define if there is a therapeutic window in which these drugs would benefit individuals with DS
436 before the appearance of toxicity. Additional research will also be required to elucidate the
437 interplay between hyperactive IFN signaling in DS with other important factors encoded on
438 chr21 (e.g. *DYRK1A*, *APP*) (Malinge et al. 2012; Wiseman et al. 2015) or elsewhere in the
439 genome, that have been involved in development of the specific comorbidities. For example, the
440 Sonic Hedgehog (SHH) pathway has been implicated in the etiology of structural and cognitive
441 defects in a mouse model of DS, including cerebellar atrophy (Das et al. 2013). Interestingly,
442 IFN signaling has been show to crosstalk with the SHH pathway, and cerebellar atrophy is also
443 a hallmark of Type I Interferonopathies (Moisan et al. 2014; Sun, Tian, and Wang 2010;
444 McGlasson et al. 2015; Crow and Manel 2015).
445 Increased JAK/STAT signaling has been postulated to contribute to some of the
446 neurological features of DS (Lee et al. 2016). Notably, it has been reported that therapeutic
447 exposure to interferons can produce diverse types of neurological dysfunction, including

448 depression, cerebral palsy and spastic diplegia (M C Wichers et al. 2005; Grether et al. 1999;
449 Wörle et al. 1999; Barlow et al. 1998). Furthermore, a large number of neurological conditions
450 have been linked to deregulated IFN signaling, most prominent among them the so called Type
451 I Interferonopathies (McGlasson et al. 2015; Crow and Manel 2015). Therefore, we propose that
452 constitutive activation of the IFN pathway in the central nervous system of individuals with DS is
453 responsible for many of the neurological problems caused by the trisomy. In particular, IFN-
454 mediated activation of microglia could lead to neurotoxicity by several mechanisms, including
455 serotonin depletion, generation of reactive oxygen species, and excitatory toxicity, which could
456 potentially be ameliorated with inhibitors of the IDO1 enzyme, a key ISG (Marieke C Wichers
457 and Maes 2004; M C Wichers et al. 2005). Although much research remains to be done, it is
458 now possible to envision early intervention strategies to ameliorate the variable ill effects of T21
459 by using pharmacological inhibitors of the IFN pathway.
460
461 **MATERIALS AND METHODS**

462 **Cell culture and drug treatments.** Six human fibroblast lines from individuals with trisomy 21
463 (T21) and six approximately age- and gender-matched fibroblast lines from typical individuals
464 (D21) were obtained from the Coriell Cell Repository and immortalized with hTERT as described
465 (Lindvall et al. 2003). EBV-immortalized lymphoblastoid lines, three T21 and three D21, were
466 obtained from the Nexus Clinical Data Registry and Biobank at the University of Colorado.
467 Fibroblasts were maintained in DMEM and lymphoblastoids were maintained in RPMI medium
468 in a humidified 5% CO_2 incubator at 37°C. Media was supplemented with 10% fetal bovine
469 serum and 1% antibiotic/antimycotic and was changed every 3-6 days. Fibroblast monolayers
470 were serially passaged by trypsin-EDTA treatment, and lymphoblastoids were serially passaged
471 via dilution in fresh media. Fibroblast lines used in this study are described in Figure 1 – figure
472 supplement 1. All cell lines were confirmed mycoplasma negative by PCR as previously

473 described (Uphoff and Drexler 2002). T21 status was authenticated as described in Figure 1 –
474 figure supplement 1D. Research Resource Identifiers (RRIDs) for fibroblast cell lines are:

Line	RRID #
GM08447	CVCL_7487
GM05659	CVCL_7434
GM00969	CVCL_7311
GM02036	CVCL_7348
GM03377	CVCL_7384
GM03440	CVCL_7388
GM04616	CVCL_V475
AG05397	CVCL_L780
AG06922	CVCL_X793
GM02767	CVCL_V469
AG08941	CVCL_X871
AG08942	CVCL_X872

475

476 **Interferon treatment in cell culture.** Recombinant human interferons alpha 2A (11101-2, R&D
477 Systems), beta (300-02BC, Peprotech) and gamma (PHC4031, Gibco) were obtained from
478 Fisher Scientific, aliquoted, and stored at -80°C. Three T21 fibroblast lines and their age- and
479 sex-matched D21 fibroblast counterparts were plated at equivalent densities and grown 72
480 hours to ensure similar cycling of the cells, then re-plated at equivalent densities and incubated
481 overnight. Media was removed the following day and replaced with media containing the
482 indicated doses of interferon ligands dissolved in PBS or vehicle (PBS alone). All media was
483 normalized for final PBS concentration at highest interferon dose. Cells were grown an
484 additional 24 hours after interferon application, then media removed, cells washed with PBS and
485 harvested via cell scraping. The harvested cells were pelleted and lysed in RIPA buffer with
486 protease and phosphatase inhibitors.
487 **JAK inhibition in cell culture.** Ruxolitinib (INCB018424) was obtained from Selleck Chemicals
488 (S1378) and dissolved in DMSO to make a 5 mM stock solution and stored at -20°C. Fibroblast
489 lines were plated at equivalent cell numbers and allowed to grow for 72 hours in order to

490 condition the media with secreted factors. Conditioned media was harvested and stored at 4°C
491 for 3-7 days prior to use. One T21 fibroblast line and its age- and sex-matched D21 fibroblast
492 counterpart were plated at equivalent cell numbers in their respective conditioned media and
493 incubated overnight. Plating media was removed the following day and replaced with
494 conditioned media containing the indicated doses of ruxolitinib or DMSO. All conditioned drug
495 media was normalized for DMSO concentration. Cells were grown an additional 72 hours after
496 drug application, harvested with trypsin-EDTA, and counted with 0.2% trypan blue using a
497 hemocytometer.
498 **Western blots.** Cells were plated at equal densities and allowed to grow 72 hours before
499 harvesting cell pellets. Pellets were washed with PBS and resuspended in RIPA buffer
500 containing 1 μg/mL pepstatin, 2 μg/mL aprotonin, 20 μg/mL trypsin inhibitor, 10 nM leupeptin,
501 200 nM Na_3VO_4, 500 nM phenylmethylsulfonyl fluoride (PMSF), and 10 μM NaF. Suspensions
502 were sonicated at six watts for 15 seconds two times and clarified by centrifugation at 21,000 g
503 for 30 minutes at 4°C. Supernatants were quantified in a Pierce BCA Protein Assay and diluted
504 in complete RIPA with 4x Laemmli sample buffer. Tris-glycine SDS-polyacrylamide gel
505 electrophoresis was used to separate 20-40 μg protein lysate, which was transferred to a 0.2
506 μm polyvinylidene fluoride (PVDF) membrane. Membranes were blocked in 5% non-fat dried
507 milk or 5% bovine serum albumin (BSA) in Tris-buffered saline containing 0.1% TWEEN (TBS-
508 T) at room temperature for 30-60 minutes before probing overnight with primary antibody in 5%
509 non-fat dried milk or 5% BSA in TBS-T at 4°C while shaking. Membranes were washed 3x in
510 TBS-T for 5-15 minutes before probing with a horseradish peroxidase (HRP) conjugated
511 secondary antibody in 5% non-fat dried milk or 5% BSA at room temperature for one hour.
512 Membranes were again washed 3x in TBS-T for 5-15 minutes before applying enhanced
513 chemiluminescence (ECL) solution. Chemiluminensence signal was captured using a GE
514 ImageQuant LAS4000.

515 Antibodies used in this study:

Antibody	Manufacturer	Product #	RRID #
anti-mouse IgG-HRP	Santa Cruz Biotechnology	sc-2005	AB_631736
anti-rabbit IgG-HRP	Santa Cruz Biotechnology	sc-2317	AB_641182
BIM	Cell Signaling Technology	2819	AB_659953
GAPDH	Santa Cruz Biotechnology	sc-365062	AB_10847862
GBP5	Abcam	ab96119	AB_10678091
IFI27	Abcam	ab171919	N/A
IFNAR1	R&D Systems	AF245	AB_355270
IFNGR2	R&D Systems	AF773	AB_355589
IL10RB	R&D Systems	AF874	AB_355677
ISG15	Cell Signaling Technology	2743	AB_2126201
MX1	Abcam	ab95926	AB_10677452
pSTAT1	Cell Signaling Technology	7649	AB_10950970
TBX21	Cell Signaling Technology	5214	AB_10692112

516

517 **Q-RT-PCR.** Total RNA was isolated using Trizol according to manufacturer's instructions. cDNA
518 was synthesized using the qScript kit from Quanta Biosciences. PCR was performed using
519 SYBR Select on a Viia7 from Life technologies.

520 Oligonucleotides used in this study:

Gene ID	Accession #	Forward	Reverse
IFI27	NM_001130080	TCTGCAGTCACTGGGAGCAACT	AACCTCGCAATGACAGCCGCAA
IFITM1	NM_003641	TTCGCTCCACGCAGAAAACCA	ACAGCCACCTCATGTTCCTCCT
MX1	NM_001144925	TCCACAGAACCGCCAAGTCCAA	ATCTGGAAGTGGAGGCGGATCA
MX2	NM_002463	TCGGACTGCAGATCAAGGCTCT	CGTGGTGGCAATGTCCACGTTA
OAS1	NM_001032409	CCGCATGCAAATCAACCATGCC	TTGCCTGAGGAGCCACCCTTTA
OAS2	NM_001032731	AGGTGGCTCCTATGGACGGAAA	CGAGGATGTCACGTTGGCTTCT

521

522 **RNA-seq from cell lines.** Biological replicates for each cell line were obtained by independently
523 growing cells in duplicate. Total RNA was purified from ~$1x10^7$ logarithmically growing cells
524 using Qiagen RNeasy columns per manufacturer's instructions including on-column DNAse
525 digestion. RNAs were quantified using a Take3 Micro-Volume plate in a Biotek Synergy2 plate
526 reader and their integrity confirmed using the Agilent RNA 6000 Pico Kit and the Agilent 2100

527 Bioanalyzer System. 500 ng of total RNA with an RNA Integrity Number (RIN) greater than 7
528 were used to prepare sequencing libraries with the Illumina TruSeq Stranded mRNA Library
529 Prep Kit. Libraries were sequenced with an Illumina HiSeq 2000 System at the UCCC
530 Genomics Core.

531 **Isolation of Monocytes and T cells by Florescence Activated Cell Sorting (FACS).**
532 Peripheral blood was collected in EDTA vacutainer tubes from 10 individuals with T21 and
533 seven D21 controls. Blood was centrifuged at 500g for 15 minutes to separate plasma, buffy
534 coat and red blood cells (RBCs). Peripheral Blood Mononuclear Cells (PBMCs) were isolated
535 from the buffy coat fraction by RBC lysis and 1x PBS wash according to manufacturer's
536 instructions (BD, 555899). After RBC lysis and PBS wash, PBMCs were stained for sorts at 10-
537 $20x10^7$ cells/ml then diluted to approximately $5x10^7$ cells/ml in flow cytometry sorting buffer (1x
538 PBS, 1 mM EDTA, 25 mM HEPES pH 7.0, 1% FBS). All staining was performed in flow
539 cytometry sorting buffer with fluorochrome-conjugated antibodies for at least 15 min on ice while
540 protected from light. Single cell suspensions were stained with CD45 (eBioscience, HI30,
541 RRID:AB_467273), CD14 (Biolegend, 63D3, RRID:AB_2571928), CD3 (Biolegend, OKT3,
542 RRID:AB_571907), CD16 (Biolegend, B73.1, RRID:AB_2616914), CD19 (Biolegend, HIB19,
543 RRID:AB_2973118), CD56 (Biolegend, 5.1H11, RRID:AB_2565855) and CD34 (Biolegend, 561,
544 RRID:AB_343601) antibodies. CD45+CD14+CD19-CD3-CD56- Monocytes and
545 CD45+CD3+CD14-CD19-CD56- T cells were FAC-sorted into Dulbecco's Modified Eagle
546 Medium (DMEM) supplemented with 4.5g/L D-Glucose, L-Glutamine, and 5% FBS, on the
547 MoFlo Astrios (Beckman Coulter) at the CU-SOM Cancer Center Flow Cytometry Shared
548 Resource.

549 **RNA extraction from Monocytes and T cells.** FAC-sorted cells were centrifuged at 500g for 5
550 minutes and media removed. Cells were resuspended in 350 μl RLT plus (QIAGEN) and Beta-
551 mercaptoethanol (BME) lysis buffer (10 μL BME:1 mL RLT plus) for downstream RNA isolation.

552 Lysed cells were immediately stored at -80°C and RNA was later extracted using the AllPrep
553 DNA/RNA/Protein Mini Kit according to manufacturer's instructions (QIAGEN, 80004). RNA
554 quality was determined by BioAnalyzer (Agilent) and quantified by Qubit (Life Technologies).
555 Samples with RIN of 7 or greater and a minimum of 500 ng total RNA were used for library prep
556 and sequencing.
557 **RNA-seq Data Analysis.** Analysis of library complexity and high per-base sequence quality
558 across all reads (i.e. q>30) was performed using FastQC (v0.11.2) software (Andrews 2010).
559 Low quality bases (q<10) were trimmed from the 3' end of reads and short reads (<30 nt after
560 trimming) and adaptor sequences were removed using the fastqc-mcf tool from ea-utils.
561 Common sources of sequence contamination such as mycoplasma, mitochondria, ribosomal
562 RNA were identified and removed using FASTQ Screen (v0.4.4). Reads were aligned to
563 GRCh37/hg19 using TopHat2 (v2.0.13, --b2-sensitive --keep-fasta-order --no-coverage-search -
564 -max-multihits 10 --library-type fr-firststrand) (D. Kim et al. 2013). High quality mapped reads
565 (MAPQ>10) were filtered with SAMtools (v0.1.19) (H. Li et al. 2009). Reads were sorted with
566 Picardtools (SortSAM) and duplicates marked (MarkDuplicates). QC of final reads was
567 performed using RSeQC (v2.6) (L. Wang, Wang, and Li 2012). Gene level counts were obtained
568 using HTSeq (v0.6.1,--stranded=reverse –minaqual=10 –type=exon –idattr=gene --mode=
569 intersection-nonempty, GTF-ftp://igenome:G3nom3s4u@ussd-
570 ftp.illumina.com/Homo_sapiens/UCSC/hg19/Homo_sapiens_UCSC_hg19.tar.gz) (Anders, Pyl,
571 and Huber 2014). Differential expression was determined using DESeq2 (v1.6.3) and R (3.10)
572 (Love, Huber, and Anders 2014). Volcano plots, manhattan plots, and violin plots, were made
573 using the Python plotting library "matplotlib" (http://matplotlib.org).
574 **shRNA Screening.** A pool of plasmids encoding 3,075 shRNAs targeting 654 kinases (kinome
575 library) in the pLKO.1 backbone produced by **T**he **R**NAi **C**onsortium (TRC, Sigma-Aldrich) were
576 obtained from the University of Colorado Cancer Center Functional Genomics Shared
577 Resource, as were the pΔ8.9 and pCMV-VSV-G lentiviral packaging plasmids. 2 μg of kinome

578 library plasmid DNA at 100 ng/μL was mixed with 2 μg of packaging plasmid mix (at a 9:1 ratio
579 of pΔ8.9:pCMV-VSV-G) at 100 ng/μL and incubated with 12 μg of Polyethylenimine for 15 min
580 at RT. The entire mixture was then added to $3x10^5$ HEK293FT packaging cells to give 100X
581 coverage. 16 h after transfection, media on cells was replaced with complete DMEM. 24 h after
582 media replacement, target cells were seeded at $1x10^5$ cells/ well in a 6-well plate. Three wells
583 for each line were combined at the time of harvest to reach a starting number of $3x10^5$ cells per
584 condition (again 100X coverage of the kinome library). 24 h after seeding, media from each well
585 of packaging cells (now containing lentiviral library particles) was filtered through 0.45 μm
586 cellulose acetate filters, diluted 1:3 into 6 mL of DMEM, and mixed with 6 μL of 8 mg/mL
587 polybrene to facilitate transduction. This mixture was then used to transduce 3 wells (one total
588 replicate) of each target cell line. 24 h after transduction viral transduction, media was replaced
589 with fresh media. Finally, after an additional 24 h, selection began by adding fresh DMEM with 1
590 μg/mL puromycin. Cells were then propagated for 14 days and genomic DNA harvested from all
591 remaining cells using the Qiagen DNeasy Blood and Tissue kit with the optional RNAse A
592 treatment step. Genomic DNA was quantified by A_{260} using a Take3 micro-volume plate on a
593 Synergy2 Microplate Reader. The quality of the genomic DNA was confirmed via
594 electrophoresis on a 0.5% TAE agarose gel. Screens were performed in three independent
595 biological replicates for each of the 12 fibroblast cell lines.
596 **shRNA Library Preparation.** The library preparation strategy uses genomic DNA and two
597 rounds of PCR in order to isolate the shRNA cassette and prepare a single strand of the hairpin
598 for sequencing by means of an XhoI restriction digest in the stem loop region. This is critical as
599 the hairpin secondary structures of shRNAs are not amenable to NGS and the TRC shRNAs do
600 not have a long enough loop to allow PCR amplification of one shRNA arm in a single step. The
601 first step in sequencing library preparation is to calculate how much genomic DNA must be used
602 for PCR1 which isolates and amplifies the shRNA cassettes from genomic DNA using Phusion

603 Polymerase. The oligonucleotides for PCR1 anneal to regions inside of the LTRs that are
604 common to all clones in the library and should, therefore, amplify all shRNA cassettes with
605 equal efficiency. Each reaction mixture for PCR1 consisted of 10 μL 5X Phusion *HF* buffer, 1 μL
606 dNTPs (10 mM each), 2.5 μL pLKO Forward and Reverse primers (10 μM), 1 μL of 2 unit/μl
607 Phusion Polymerase, 500 ng genomic DNA, and dH2O to 50 μL. The cycling conditions were as
608 follows: 1 cycle of 98°C for 5 min, 15 to 25 cycles of 98°C for 30 s, 70°C for 30 s, 72°C for 30 s,
609 and 1 cycle of 72°C for 7 min. 5 μL of each PCR1 were run on a 2% TAE agarose gel in order to
610 visualize the expected band of 497 bp. It should be noted that optimal PCR1 cycle number must
611 be empirically determined for each library and to limit cycle numbers to minimize the effects of
612 amplification bias. The correct product of PCR1 is 497 bp; however, excessive cycle numbers
613 can result in the appearance of a slower migrating band. This band represents an annealing
614 event between two amplification products with different shRNA sequences. As the majority of
615 the 497 bp amplicon is common to all products, denatured PCR products can anneal to one
616 another when not out-competed by an excess of primer in later cycles. This aberrant product
617 does not correctly anneal within the central shRNA-containing sequence, therefore disrupting
618 the double-stranded XhoI site required for the subsequent restriction digestion. Carefully
619 determining the appropriate number of cycles prevents the appearance of this undesired
620 product. After establishing optimal cycle number, we performed 12 identical PCR1 reactions in
621 order to amplify sufficient amounts of genomic DNA and pooled them all prior to cleanup with a
622 QIAquick PCR Purification Kit.
623 **XhoI digest.** 1 μg of the resulting DNA was digested with XhoI overnight at 37°C. Digest
624 reactions consisted of 3.5 μL 10X FD buffer, 1 μL of 20,000 units/mL XhoI, 1 μg of DNA and
625 dH2O to 35 μL. Heat inactivation of XhoI is not recommended, as the high temperatures result
626 in reappearance of the spurious annealing products mentioned above, leading to a disruption of
627 the XhoI overhang required for ligation. For the TRC1 and TRC1.5 libraries, there are two XhoI

628 sites within the product of PCR1, resulting in fragments of 271, 43 and 183 bp. In order to purify
629 the desired fragment, the entire digest was run on a 2% TAE agarose gel and purified the 271
630 bp fragment using a QIAquick Gel Extraction Kit. Once the band was excised, three volumes of
631 buffer QG were added and the mixture heated at 30°C to dissolve the agarose. Lower melting
632 temperatures are recommended so as not to denature the complementary double-stranded
633 shRNA cassettes, which may not reanneal to their cognate strand. After the agarose was
634 dissolved, one volume of isopropanol was added and protocol resumed following the
635 manufacturer's instructions including the optional addition of NaOAc.
636 **Ligation of barcoded linkers.** We prepared the barcoded linkers required for ligation by
637 resuspending the lyophilized oligonucleotides in ST buffer (10 mM Tris pH 8.0, 50 mM NaCl) to
638 200 μM and combining 25 μL of each for a final concentration of 100 μM. The mixture was
639 heated to 94°C for 10 min and gradually cooled to ensure proper annealing. Single-stranded
640 oligonucleotides were removed from annealed oligonucleotides using Illustra MicroSpin G-25
641 columns. The sense (S1-S4) oligonucleotides are 5'-phosphorylated and the antisense
642 oligonucleotides (AS1-AS4) each contain a single phosphorothioate bond at the 3' end to
643 stabilize them and are designed to prevent the reformation of a functional XhoI site. The
644 barcodes within these linkers are used for multiplexing and their length ensures they are
645 compatible with the Illumina HiSeq 2000. Shorter barcode sequences may be compatible with
646 other sequencing platforms. The selected barcoded linkers were added to ligation reactions with
647 100 ng of each purified 271 bp XhoI fragment, 3.5 μL 10X T4 DNA ligase buffer, 4 μL of 1 μM
648 barcoded linker, 1 μL T4 DNA ligase and dH_2O to 35 μL. Ligations were performed overnight at
649 16°C. The entire ligation was run on a 2% TAE agarose gel and the resulting 312 bp band
650 purified using the QIAquick Gel Extraction Kit in the same manner as previously described.
651 **PCR2.** The final step in the preparation of the sequencing library is a second PCR with
652 oligonucleotides that contain the Illumina adaptors required for bridge amplification and

653 sequencing. In this PCR, the number of cycles is minimized in order to avoid PCR bias as well
654 as errors that could affect sequencing. The reaction for PCR2 was as follows: 10 μL 5X Phusion
655 HF buffer, 1 μL dNTPs (10 mM each), 2.5 μL Forward adapter primer (10 μM) 2.5 μL, Reverse
656 adapter primer (10 μM), 1 μL Phusion DNA polymerase 10 ng barcoded DNA, and dH_2O to 50
657 μL. The cycling program consisted of 1 cycle of 98°C for 2 min, 2 cycles of 98°C for 30 s, 62°C
658 for 30 s, 72°C for 30 s, 7 cycles of 98°C for 30 s, 72°C for 30 s and 1 cycle of 72°C for 3 min.
659 The final 141 bp product was purified on a 2% TAE-agarose gel followed by QIAquick Gel
660 Extraction as described above.
661 **Illumina Sequencing.** We assessed the purity of our sequencing library using the Bioanalyzer
662 High Sensitivity DNA Kit (Agilent-5067-4626) and confirmed the presence of a single 141 bp
663 peak, indicating one PCR product at the appropriate size. We utilized a multiplexing strategy
664 consisting of four different barcodes with each nucleotide represented at each position of the
665 barcode, allowing us to sequence four samples in each lane on a HiSeq 2000 Illumina
666 instrument. To accomplish this, each sample was quantified and mixed together at a final
667 concentration of 10 ng/μL and using Illumina-specific oligonucleotides and qPCR, we
668 determined the cluster formation efficiency (i.e. effective concentration) of our library to be
669 slightly greater than that of a known library. Accordingly, we loaded the flow cell at 5 pM and
670 included a 10% ΦX-174 spike-in, which aids in quality control of cluster formation and
671 sequencing on the Illumina platform. Cluster formation efficiency and the concentration of library
672 to be loaded on the flow cell needs to be determined empirically for each library preparation.
673 These loading conditions yielded cluster densities between 733,000 clusters/mm^2 and 802,000
674 clusters/mm^2 and between 203 and 222 million reads per lane.
675 **shRNA Screen Analysis.** shRNA data were analyzed in a similar fashion to RNA-seq data.
676 Briefly, quality control was performed with FastQC, reads were trimmed to include only shRNA
677 sequences using FASTQ trimmer, and filtered with the FASTQ Quality Filter. Reads were then

678 aligned to a custom reference library of shRNA sequences using TopHat2. Three out of 36
679 samples were removed based on poor performance in unsupervised hierarchical clustering
680 and/or principal component analysis, but each fibroblast cell line retained at least two biological
681 replicates and nine of 12 retained all three replicates. Count tables were generated using
682 HTSeq and differential expression determined by DESeq2.
683 **SOMAScan proteomics.** Cell lysates from all 12 fibroblast cell lines were analyzed using
684 SOMAscan v4.0 according to manufacturer's instructions and as previously reported (Hathout et
685 al. 2015; Mehan et al. 2014). Data were analyzed using the QPROT statistical package (Choi et
686 al. 2015).
687 **Isolation of RNA from LSK cells for RNA-seq.** Whole bone marrow was harvested from the
688 long bones of Dp16 mice (RRID:IMSR_JAX:013530) and matched littermate controls. Cells
689 were first purified using hemolysis to remove RBCs and then stained and sorted for LSK cells
690 (CD3-, Ter119-, Mac1-, Gr1-, B220-, Sca1+, cKit) using the Moflo XDP 70 FACS sorter. RNA
691 was then isolated from these cells using the RNeasy Kit from Qiagen.
692 **Acknowledgements.** This work was supported primarily by the Linda Crnic Institute for Down
693 Syndrome and the Anna and John J. Sie Foundation. We thank T. Blumenthal and J. Costello
694 for stimulating discussion and critical reading of this manuscript. We also thank the individuals
695 with Down syndrome that donated the biological samples that enabled these studies. We also
696 thank the Functional Genomics, Genomics, and Flow Cytometry Shared Resources at the
697 University of Colorado Cancer Center.
698
699 **ADDITIONAL INFORMATION**
700 **Competing interests.** JME: Reviewing Editor, eLife. The other authors declare no competing
701 interests.
702 **Funding.** This work was supported primarily by the Linda Crnic Institute for Down Syndrome
703 and the Anna and John J. Sie Foundation, and also by NIH grants R01CA117907 and

704 P30CA046934-27, NSF Grant MCB-1243522, and the Howard Hughes Medical Institute.

705 **Author Contributions.** KDS and JME, conception and design, acquisition of data, analysis and
706 interpretation of data, drafting or revising the article; HCL, AAH, KPS, LPJ, AL, JD, EBG, JMC,
707 conception and design, acquisition of data, analysis and interpretation of data; AP and MDG,
708 Analysis and interpretation of data.
709

710 **REFERENCES**

711 Ahmed, Md Mahiuddin, A Ranjitha Dhanasekaran, Suhong Tong, Frances K Wiseman,
712 Elizabeth M C Fisher, Victor L J Tybulewicz, and Katheleen J Gardiner. 2013. "Protein
713 Profiles in Tc1 Mice Implicate Novel Pathway Perturbations in the Down Syndrome Brain."
714 *Human Molecular Genetics* 22 (9): 1709–24. doi:10.1093/hmg/ddt017.

715 Alexander, Myriam, Hans Petri, Yingjie Ding, Christoph Wandel, Omar Khwaja, and Nadia
716 Foskett. 2016. "Morbidity and Medication in a Large Population of Individuals with Down
717 Syndrome Compared to the General Population." *Developmental Medicine and Child*
718 *Neurology* 58 (3): 246–54. doi:10.1111/dmcn.12868.

719 Anders, Simon, Paul Theodor Pyl, and Wolfgang Huber. 2014. "HTSeq - A Python Framework
720 to Work with High-Throughput Sequencing Data." *Bioinformatics (Oxford, England)* 31 (2):
721 166–69. doi:10.1093/bioinformatics/btu638.

722 Andrews, Simon. 2010. "FastQC: A Quality Control Tool for High Throughput Sequence Data."
723 *Http://www.bioinformatics.babraham.ac.uk/projects/fastqc/*.

724 Anwar, A J, J D Walker, and B M Frier. 1998. "Type 1 Diabetes Mellitus and Down's Syndrome:
725 Prevalence, Management and Diabetic Complications." *Diabetic Medicine : A Journal of the*
726 *British Diabetic Association* 15 (2): 160–63. doi:10.1002/(SICI)1096-
727 9136(199802)15:2<160::AID-DIA537>3.0.CO;2-J.

728 Arabi, Azadeh, Siqin Wu, Karin Ridderstråle, Holger Bierhoff, Chiounan Shiue, Karoly Fatyol,
729 Sara Fahlén, et al. 2005. "C-Myc Associates with Ribosomal DNA and Activates RNA
730 Polymerase I Transcription." *Nature Cell Biology* 7 (3): 303–10. doi:10.1038/ncb1225.

731 Barlow, Charles F., Cedric J. Priebe, John B. Mulliken, Patrick D. Barnes, Dorothy Mac Donald,
732 Judah Folkman, and R.Alan B. Ezekowitz. 1998. "Spastic Diplegia as a Complication of
733 Interferon Alfa-2a Treatment of Hemangiomas of Infancy." *The Journal of Pediatrics* 132
734 (3): 527–30. doi:10.1016/S0022-3476(98)70034-4.

735 Boon, K, H N Caron, R van Asperen, L Valentijn, M C Hermus, P van Sluis, I Roobeek, et al.

736 2001. “N-Myc Enhances the Expression of a Large Set of Genes Functioning in Ribosome
737 Biogenesis and Protein Synthesis.” *The EMBO Journal* 20 (6): 1383–93.
738 doi:10.1093/emboj/20.6.1383.
739 Bratman, Scott V, Kathleen C Horst, Robert W Carlson, and Daniel S Kapp. 2014. “Solid
740 Malignancies in Individuals with Down Syndrome: A Case Presentation and Literature
741 Review.” *Journal of the National Comprehensive Cancer Network : JNCCN* 12 (11): 1537–
742 45.
743 Cerami, Ethan G, Benjamin E Gross, Emek Demir, Igor Rodchenkov, Ozgün Babur, Nadia
744 Anwar, Nikolaus Schultz, Gary D Bader, and Chris Sander. 2011. “Pathway Commons, a
745 Web Resource for Biological Pathway Data.” *Nucleic Acids Research* 39 (Database issue):
746 D685–90. doi:10.1093/nar/gkq1039.
747 Choi, Hyungwon, Sinae Kim, Damian Fermin, Chih-Chiang Tsou, and Alexey I. Nesvizhskii.
748 2015. “QPROT: Statistical Method for Testing Differential Expression Using Protein-Level
749 Intensity Data in Label-Free Quantitative Proteomics.” *Journal of Proteomics* 129: 121–26.
750 doi:10.1016/j.jprot.2015.07.036.
751 Costa, Valerio, Claudia Angelini, Luciana D’Apice, Margherita Mutarelli, Amelia Casamassimi,
752 Linda Sommese, Maria Assunta Gallo, et al. 2011. “Massive-Scale RNA-Seq Analysis of
753 Non Ribosomal Transcriptome in Human Trisomy 21.” *PloS One* 6 (4). Public Library of
754 Science: e18493. doi:10.1371/journal.pone.0018493.
755 Crow, Yanick J, and Nicolas Manel. 2015. “Aicardi-Goutières Syndrome and the Type I
756 Interferonopathies.” *Nature Reviews. Immunology* 15 (7). Nature Publishing Group, a
757 division of Macmillan Publishers Limited. All Rights Reserved.: 429–40.
758 doi:10.1038/nri3850.
759 Das, Ishita, Joo-Min Park, Jung H Shin, Soo Kyeong Jeon, Hernan Lorenzi, David J Linden,
760 Paul F Worley, et al. 2013. “Hedgehog Agonist Therapy Corrects Structural and Cognitive
761 Deficits in a Down Syndrome Mouse Model.” *Science Translational Medicine* 5 (201).

762 American Association for the Advancement of Science: 201ra120.
763 doi:10.1126/scitranslmed.3005983.
764 de Sola, Susana, Rafael de la Torre, Gonzalo Sánchez-Benavides, Bessy Benejam, Aida
765 Cuenca-Royo, Laura Del Hoyo, Joan Rodríguez, et al. 2015. "A New Cognitive Evaluation
766 Battery for Down Syndrome and Its Relevance for Clinical Trials." *Frontiers in Psychology* 6
767 (January): 708. doi:10.3389/fpsyg.2015.00708.
768 Do, Long H, William C Mobley, and Nishant Singhal. 2015. "Questioned Validity of Gene
769 Expression Dysregulated Domains in Down's Syndrome." *F1000Research* 4 (January):
770 269. doi:10.12688/f1000research.6735.1.
771 Donner, Aaron J, Christopher C Ebmeier, Dylan J Taatjes, and Joaquín M Espinosa. 2010.
772 "CDK8 Is a Positive Regulator of Transcriptional Elongation within the Serum Response
773 Network." *Nature Structural & Molecular Biology* 17 (2): 194–201. doi:10.1038/nsmb.1752.
774 Galbraith, Matthew D, Mary A Allen, Claire L Bensard, Xiaoxing Wang, Marie K Schwinn, Bo
775 Qin, Henry W Long, et al. 2013. "HIF1A Employs CDK8-Mediator to Stimulate RNAPII
776 Elongation in Response to Hypoxia." *Cell* 153 (6): 1327–39. doi:10.1016/j.cell.2013.04.048.
777 Gold, Larry, Jeffrey J Walker, Sheri K Wilcox, and Stephen Williams. 2012. "Advances in
778 Human Proteomics at High Scale with the SOMAscan Proteomics Platform." *New
779 Biotechnology* 29 (5): 543–49. doi:10.1016/j.nbt.2011.11.016.
780 Grether, Judith K., Karin B. Nelson, James M. Dambrosia, and Terry M. Phillips. 1999.
781 "Interferons and Cerebral Palsy." *The Journal of Pediatrics* 134 (3): 324–32.
782 doi:10.1016/S0022-3476(99)70458-0.
783 Gupta, Rahul, Sun Kim, Milton W Taylor, JB Wong, GM McQuillan, JG McHutchison, T
784 Poynard, et al. 2012. "Suppression of Ribosomal Protein Synthesis and Protein Translation
785 Factors by Peg-Interferon Alpha/ribavirin in HCV Patients Blood Mononuclear Cells
786 (PBMC)." *Journal of Translational Medicine* 10 (1). BioMed Central: 54. doi:10.1186/1479-
787 5876-10-54.

788 Hasle, Henrik, Jan M. Friedman, Jørgen H. Olsen, and Sonja A. Rasmussen. 2016. “Low Risk
789 of Solid Tumors in Persons with Down Syndrome.” *Genetics in Medicine*, March. Nature
790 Publishing Group. doi:10.1038/gim.2016.23.
791 Hathout, Yetrib, Edward Brody, Paula R Clemens, Linda Cripe, Robert Kirk DeLisle, Pat
792 Furlong, Heather Gordish-Dressman, et al. 2015. “Large-Scale Serum Protein Biomarker
793 Discovery in Duchenne Muscular Dystrophy.” *Proceedings of the National Academy of*
794 *Sciences of the United States of America* 112 (23): 7153–58.
795 doi:10.1073/pnas.1507719112.
796 Hinnebusch, Alan G. 2014. “The Scanning Mechanism of Eukaryotic Translation Initiation.”
797 *Annual Review of Biochemistry* 83: 779–812. doi:10.1146/annurev-biochem-060713-
798 035802.
799 Huang, Chen, Li-Ying Liu, Zong-Fang Li, Pei Wang, Lei Ni, Li-Ping Song, De-Hui Xu, and Tu-
800 Sheng Song. 2008. “Effects of Small Interfering RNAs Targeting MAPK1 on Gene
801 Expression Profile in HeLa Cells as Revealed by Microarray Analysis.” *Cell Biology*
802 *International* 32 (9): 1081–90. doi:10.1016/j.cellbi.2008.04.019.
803 Iwamoto, Tsutomu, Aya Yamada, Kenji Yuasa, Emiko Fukumoto, Takashi Nakamura, Taku
804 Fujiwara, and Satoshi Fukumoto. 2009. “Influences of Interferon-Gamma on Cell
805 Proliferation and Interleukin-6 Production in Down Syndrome Derived Fibroblasts.”
806 *Archives of Oral Biology* 54 (10): 963–69. doi:10.1016/j.archoralbio.2009.07.009.
807 Iyer, Anand M, Jackelien van Scheppingen, Ivan Milenkovic, Jasper J Anink, Homa Adle-
808 Biassette, Gabor G Kovacs, and Eleonora Aronica. 2014. “mTOR Hyperactivation in down
809 Syndrome Hippocampus Appears Early during Development.” *Journal of Neuropathology*
810 *and Experimental Neurology* 73 (7): 671–83. doi:10.1097/NEN.0000000000000083.
811 Jabbari, Ali, Zhenpeng Dai, Luzhou Xing, Jane E Cerise, Yuval Ramot, Yackov Berkun, Gina A
812 Montealegre Sanchez, et al. 2015. “Reversal of Alopecia Areata Following Treatment With
813 the JAK1/2 Inhibitor Baricitinib.” *EBioMedicine* 2 (4): 351–55.

814 doi:10.1016/j.ebiom.2015.02.015.
815 Johnson, T C, M P Lerner, and G J Lancz. 1968. “Inhibition of Protein Synthesis in Noninfected
816 L Cells by Partially Purified Interferon Preparations.” *The Journal of Cell Biology* 36 (3):
817 617–24.
818 Keystone, Edward C, Peter C Taylor, Edit Drescher, Douglas E Schlichting, Scott D Beattie,
819 Pierre-Yves Berclaz, Chin H Lee, et al. 2015. “Safety and Efficacy of Baricitinib at 24
820 Weeks in Patients with Rheumatoid Arthritis Who Have Had an Inadequate Response to
821 Methotrexate.” *Annals of the Rheumatic Diseases* 74 (2): 333–40.
822 doi:10.1136/annrheumdis-2014-206478.
823 Kim, Daehwan, Geo Pertea, Cole Trapnell, Harold Pimentel, Ryan Kelley, and Steven L
824 Salzberg. 2013. “TopHat2: Accurate Alignment of Transcriptomes in the Presence of
825 Insertions, Deletions and Gene Fusions.” *Genome Biology* 14 (4). BioMed Central: R36.
826 doi:10.1186/gb-2013-14-4-r36.
827 Kim, S, Q Li, C V Dang, and L A Lee. 2000. “Induction of Ribosomal Genes and Hepatocyte
828 Hypertrophy by Adenovirus-Mediated Expression of c-Myc in Vivo.” *Proceedings of the*
829 *National Academy of Sciences of the United States of America* 97 (21): 11198–202.
830 doi:10.1073/pnas.200372597.
831 Krämer, Andreas, Jeff Green, Jack Pollard, and Stuart Tugendreich. 2014. “Causal Analysis
832 Approaches in Ingenuity Pathway Analysis.” *Bioinformatics (Oxford, England)* 30 (4): 523–
833 30. doi:10.1093/bioinformatics/btt703.
834 Lee, Han-Chung, Kai-Leng Tan, Pike-See Cheah, and King-Hwa Ling. 2016. “Potential Role of
835 JAK-STAT Signaling Pathway in the Neurogenic-to-Gliogenic Shift in Down Syndrome
836 Brain.” *Neural Plasticity* 2016 (January): 7434191. doi:10.1155/2016/7434191.
837 Letourneau, Audrey, Federico A Santoni, Ximena Bonilla, M Reza Sailani, David Gonzalez, Jop
838 Kind, Claire Chevalier, et al. 2014. “Domains of Genome-Wide Gene Expression
839 Dysregulation in Down’s Syndrome.” *Nature* 508 (7496). Nature Publishing Group, a

840 division of Macmillan Publishers Limited. All Rights Reserved.: 345–50.
841 doi:10.1038/nature13200.
842 Li, Heng, Bob Handsaker, Alec Wysoker, Tim Fennell, Jue Ruan, Nils Homer, Gabor Marth,
843 Goncalo Abecasis, and Richard Durbin. 2009. “The Sequence Alignment/Map Format and
844 SAMtools.” *Bioinformatics (Oxford, England)* 25: 2078–79.
845 doi:10.1093/bioinformatics/btp352.
846 Li, Zhongyou, Tao Yu, Masae Morishima, Annie Pao, Jeffrey LaDuca, Jeffrey Conroy, Norma
847 Nowak, Sei-Ichi Matsui, Isao Shiraishi, and Y Eugene Yu. 2007. “Duplication of the Entire
848 22.9 Mb Human Chromosome 21 Syntenic Region on Mouse Chromosome 16 Causes
849 Cardiovascular and Gastrointestinal Abnormalities.” *Human Molecular Genetics* 16 (11):
850 1359–66. doi:10.1093/hmg/ddm086.
851 Lindvall, Charlotta, Mi Hou, Toshi Komurasaki, Chengyun Zheng, Marie Henriksson, John M.
852 Sedivy, Magnus Bjorkholm, Bin Tean Teh, Magnus Nordenskjold, and Dawei Xu. 2003.
853 “Molecular Characterization of Human Telomerase Reverse Transcriptase-Immortalized
854 Human Fibroblasts by Gene Expression Profiling: Activation of the Epiregulin Gene.”
855 *Cancer Res.* 63 (8): 1743–47.
856 Ling, King-Hwa, Chelsee A Hewitt, Kai-Leng Tan, Pike-See Cheah, Sharmili Vidyadaran, Mei-I
857 Lai, Han-Chung Lee, et al. 2014. “Functional Transcriptome Analysis of the Postnatal Brain
858 of the Ts1Cje Mouse Model for Down Syndrome Reveals Global Disruption of Interferon-
859 Related Molecular Networks.” *BMC Genomics* 15 (1): 624. doi:10.1186/1471-2164-15-624.
860 Love, Michael I, Wolfgang Huber, and Simon Anders. 2014. “Moderated Estimation of Fold
861 Change and Dispersion for RNA-Seq Data with DESeq2.” *Genome Biology* 15 (12): 550.
862 doi:10.1186/PREACCEPT-8897612761307401.
863 Malinge, Sébastien, Meghan Bliss-Moreau, Gina Kirsammer, Lauren Diebold, Timothy Chlon,
864 Sandeep Gurbuxani, and John D Crispino. 2012. “Increased Dosage of the Chromosome
865 21 Ortholog Dyrk1a Promotes Megakaryoblastic Leukemia in a Murine Model of Down

866 Syndrome." *The Journal of Clinical Investigation* 122 (3): 948–62. doi:10.1172/JCI60455.
867 Malinge, Sébastien, Tim Chlon, Louis C Doré, Rhett P Ketterling, Martin S Tallman, Elisabeth
868 Paietta, Alan S Gamis, et al. 2013. "Development of Acute Megakaryoblastic Leukemia in
869 Down Syndrome Is Associated with Sequential Epigenetic Changes." *Blood* 122 (14): e33–
870 43. doi:10.1182/blood-2013-05-503011.
871 Maroun, L E. 1978. "Interferon-Mediated Effect on Ribosomal RNA Metabolism." *Biochimica et*
872 *Biophysica Acta* 517 (1): 109–14.
873 ———. 1995. "Anti-Interferon Immunoglobulins Can Improve the Trisomy 16 Mouse
874 Phenotype." *Teratology* 51 (5): 329–35. doi:10.1002/tera.1420510509.
875 Maroun, L E, T N Heffernan, and D M Hallam. 2000. "Partial IFN-Alpha/beta and IFN-Gamma
876 Receptor Knockout Trisomy 16 Mouse Fetuses Show Improved Growth and Cultured
877 Neuron Viability." *Journal of Interferon & Cytokine Research : The Official Journal of the*
878 *International Society for Interferon and Cytokine Research* 20 (2): 197–203.
879 doi:10.1089/107999000312612.
880 McGlasson, Sarah, Alexa Jury, Andrew Jackson, and David Hunt. 2015. "Type I Interferon
881 Dysregulation and Neurological Disease." *Nature Reviews. Neurology* 11 (9): 515–23.
882 doi:10.1038/nrneurol.2015.143.
883 McKeage, Kate. 2015. "Ruxolitinib: A Review in Polycythaemia Vera." *Drugs* 75 (15): 1773–81.
884 doi:10.1007/s40265-015-0470-2.
885 Mehan, Michael R, Stephen A Williams, Jill M Siegfried, William L Bigbee, Joel L Weissfeld,
886 David O Wilson, Harvey I Pass, et al. 2014. "Validation of a Blood Protein Signature for
887 Non-Small Cell Lung Cancer." *Clinical Proteomics* 11 (1): 32. doi:10.1186/1559-0275-11-
888 32.
889 Moisan, Annie, Youn-Kyoung Lee, Jitao David Zhang, Carolyn S. Hudak, Claas A. Meyer,
890 Michael Prummer, Sannah Zoffmann, et al. 2014. "White-to-Brown Metabolic Conversion of
891 Human Adipocytes by JAK Inhibition." *Nature Cell Biology* 17 (1). Nature Publishing Group:

892 57–67. doi:10.1038/ncb3075.
893 Müller, M, J Briscoe, C Laxton, D Guschin, A Ziemiecki, O Silvennoinen, A G Harpur, G
894 Barbieri, B A Witthuhn, and C Schindler. 1993. “The Protein Tyrosine Kinase JAK1
895 Complements Defects in Interferon-Alpha/beta and -Gamma Signal Transduction.” *Nature*
896 366 (6451): 129–35. doi:10.1038/366129a0.
897 Padron, Eric, Amy Dezern, Marcio Andrade-Campos, Kris Vaddi, Peggy Scherle, Qing Zhang,
898 Yan Ma, et al. 2016. “A Multi-Institution Phase 1 Trial of Ruxolitinib in Patients with Chronic
899 Myelomonocytic Leukemia (CMML).” *Clinical Cancer Research : An Official Journal of the*
900 *American Association for Cancer Research*, February. Clinical Cancer Research,
901 clincanres.2781.2015. doi:10.1158/1078-0432.CCR-15-2781.
902 Perluigi, Marzia, Fabio Di Domenico, and D Allan Butterfield. 2015. “mTOR Signaling in Aging
903 and Neurodegeneration: At the Crossroad between Metabolism Dysfunction and
904 Impairment of Autophagy.” *Neurobiology of Disease* 84 (March): 39–49.
905 doi:10.1016/j.nbd.2015.03.014.
906 Plosker, Greg L. 2015. “Ruxolitinib: A Review of Its Use in Patients with Myelofibrosis.” *Drugs*
907 75 (3): 297–308. doi:10.1007/s40265-015-0351-8.
908 Quintás-Cardama, Alfonso, Kris Vaddi, Phillip Liu, Taghi Manshouri, Jun Li, Peggy A Scherle,
909 Eian Caulder, et al. 2010. “Preclinical Characterization of the Selective JAK1/2 Inhibitor
910 INCB018424: Therapeutic Implications for the Treatment of Myeloproliferative Neoplasms.”
911 *Blood* 115 (15): 3109–17. doi:10.1182/blood-2009-04-214957.
912 Richardson, Sarah J., Abby Willcox, Adrian J. Bone, Noel G. Morgan, and Alan K. Foulis. 2010.
913 “Immunopathology of the Human Pancreas in Type-I Diabetes.” *Seminars in*
914 *Immunopathology* 33 (1): 9–21. doi:10.1007/s00281-010-0205-0.
915 Roberts, Irene, and Shai Izraeli. 2014. “Haematopoietic Development and Leukaemia in Down
916 Syndrome.” *British Journal of Haematology* 167 (5): 587–99. doi:10.1111/bjh.13096.
917 Scarpato, Margherita, Roberta Esposito, Daniela Evangelista, Marianna Aprile, Maria Rosaria

Ambrosio, Claudia Angelini, Alfredo Ciccodicola, and Valerio Costa. 2014. “AnaLysis of Expression on Human Chromosome 21, ALE-HSA21: A Pilot Integrated Web Resource.” *Database : The Journal of Biological Databases and Curation* 2014 (0): bau009. doi:10.1093/database/bau009.

Schoggins, John W, Sam J Wilson, Maryline Panis, Mary Y Murphy, Christopher T Jones, Paul Bieniasz, and Charles M Rice. 2011. “A Diverse Range of Gene Products Are Effectors of the Type I Interferon Antiviral Response.” *Nature* 472 (7344): 481–85. doi:10.1038/nature09907.

Shi, Jack G., Xuejun Chen, Fiona Lee, Thomas Emm, Peggy A. Scherle, Yvonne Lo, Naresh Punwani, William V. Williams, and Swamy Yeleswaram. 2014. “The Pharmacokinetics, Pharmacodynamics, and Safety of Baricitinib, an Oral JAK 1/2 Inhibitor, in Healthy Volunteers.” *The Journal of Clinical Pharmacology* 54 (12): 1354–61. doi:10.1002/jcph.354.

Shuai, K, Curt M. Horvath, Linda H.Tsai Huang, Sajjad A. Qureshi, David Cowburn, and James E. Darnell. 1994. “Interferon Activation of the Transcription Factor Stat91 Involves Dimerization through SH2-Phosphotyrosyl Peptide Interactions.” *Cell* 76 (5). Cell Press: 821–28. doi:10.1016/0092-8674(94)90357-3.

Slate, D L, L Shulman, J B Lawrence, M Revel, and F H Ruddle. 1978. “Presence of Human Chromosome 21 Alone Is Sufficient for Hybrid Cell Sensitivity to Human Interferon.” *Journal of Virology* 25 (1): 319–25.

Sobey, Christopher G, Courtney P Judkins, Vijaya Sundararajan, Thanh G Phan, Grant R Drummond, and Velandai K Srikanth. 2015. “Risk of Major Cardiovascular Events in People with Down Syndrome.” *PloS One* 10 (9): e0137093. doi:10.1371/journal.pone.0137093.

Spaner, David E, Guizhei Wang, Lindsay McCaw, Yanmei Li, Patricia Disperati, Mary-Ann Cussen, and Yonghong Shi. 2016. “Activity of the Janus Kinase Inhibitor Ruxolitinib in Chronic Lymphocytic Leukemia: Results of a Phase II Trial.” *Haematologica* 101 (5): e192–

95. doi:10.3324/haematol.2015.135418.

Stahl, N, T G Boulton, T Farruggella, N Y Ip, S Davis, B A Witthuhn, F W Quelle, O Silvennoinen, G Barbieri, and S Pellegrini. 1994. “Association and Activation of Jak-Tyk Kinases by CNTF-LIF-OSM-IL-6 Beta Receptor Components.” *Science (New York, N.Y.)* 263 (5143): 92–95.

Stankiewicz, M J, and J D Crispino. 2013. “AKT Collaborates with ERG and Gata1s to Dysregulate Megakaryopoiesis and Promote AMKL.” *Leukemia* 27 (6): 1339–47. doi:10.1038/leu.2013.33.

Sullivan, Kelly D, Nuria Padilla-Just, Ryan E Henry, Christopher C Porter, Jihye Kim, John J Tentler, S Gail Eckhardt, Aik Choon Tan, James DeGregori, and Joaquín M Espinosa. 2012. “ATM and MET Kinases Are Synthetic Lethal with Nongenotoxic Activation of p53.” *Nature Chemical Biology* 8 (7): 646–54. doi:10.1038/nchembio.965.

Sun, Li, Zhanzhuang Tian, and Jianping Wang. 2010. “A Direct Cross-Talk between Interferon-γ and Sonic Hedgehog Signaling That Leads to the Proliferation of Neuronal Precursor Cells.” *Brain, Behavior, and Immunity* 24 (2): 220–28. doi:10.1016/j.bbi.2009.09.016.

Tan, Y H, E L Schneider, J Tischfield, C J Epstein, and F H Ruddle. 1974. “Human Chromosome 21 Dosage: Effect on the Expression of the Interferon Induced Antiviral State.” *Science (New York, N.Y.)* 186 (4158): 61–63.

Tan, Y H, J A Tischfield, and F H Ruddle. 1974. “Proceedings: The Genetics of the Antiviral State in Human Cells.” *Cytogenetics and Cell Genetics* 13 (1): 158–59.

Tanaka, Marcia H, Elisa M A Giro, Lícia B Cavalcante, Juliana R Pires, Luciano H Apponi, Sandro R Valentini, Denise M P Spolidório, Marisa V Capela, Carlos Rossa, and Raquel M Scarel-Caminaga. 2012. “Expression of Interferon-Γ, Interferon-α and Related Genes in Individuals with Down Syndrome and Periodontitis.” *Cytokine* 60 (3): 875–81. doi:10.1016/j.cyto.2012.08.020.

Taylor, Milton W, Takuma Tsukahara, Leonid Brodsky, Joel Schaley, Corneliu Sanda, Matthew

970 J Stephens, Jeanette N McClintick, et al. 2007. “Changes in Gene Expression during
971 Pegylated Interferon and Ribavirin Therapy of Chronic Hepatitis C Virus Distinguish
972 Responders from Nonresponders to Antiviral Therapy.” *Journal of Virology* 81 (7).
973 American Society for Microbiology (ASM): 3391–3401. doi:10.1128/JVI.02640-06.
974 Tefferi, Ayalew, Mark R Litzow, and Animesh Pardanani. 2011. “Long-Term Outcome of
975 Treatment with Ruxolitinib in Myelofibrosis.” *The New England Journal of Medicine* 365
976 (15): 1455–57. doi:10.1056/NEJMc1109555.
977 Tisserand, Johan, Konstantin Khetchoumian, Christelle Thibault, Doulaye Dembélé, Pierre
978 Chambon, and Régine Losson. 2011. “Tripartite Motif 24 (Trim24/Tif1α) Tumor Suppressor
979 Protein Is a Novel Negative Regulator of Interferon (IFN)/signal Transducers and Activators
980 of Transcription (STAT) Signaling Pathway Acting through Retinoic Acid Receptor α (Rarα)
981 Inhibition.” *The Journal of Biological Chemistry* 286 (38): 33369–79.
982 doi:10.1074/jbc.M111.225680.
983 Troca-Marín, Jose Antonio, Juan José Casañas, Itziar Benito, and María Luz Montesinos. 2014.
984 “The Akt-mTOR Pathway in Down’s Syndrome: The Potential Use of Rapamycin/rapalogs
985 for Treating Cognitive Deficits.” *CNS & Neurological Disorders Drug Targets* 13 (1): 34–40.
986 Uphoff, C C, and H G Drexler. 2002. “Detection of Mycoplasma in Leukemia-Lymphoma Cell
987 Lines Using Polymerase Chain Reaction.” *Leukemia* 16 (2): 289–93.
988 doi:10.1038/sj.leu.2402365.
989 van Riggelen, Jan, Alper Yetil, and Dean W Felsher. 2010. “MYC as a Regulator of Ribosome
990 Biogenesis and Protein Synthesis.” *Nature Reviews. Cancer* 10 (4): 301–9.
991 doi:10.1038/nrc2819.
992 Volk, Marija, Aleš Maver, Luca Lovrečić, Peter Juvan, and Borut Peterlin. 2013. “Expression
993 Signature as a Biomarker for Prenatal Diagnosis of Trisomy 21.” *PloS One* 8 (9). Public
994 Library of Science: e74184. doi:10.1371/journal.pone.0074184.
995 Waddell, Simon J, Stephen J Popper, Kathleen H Rubins, Michael J Griffiths, Patrick O Brown,

996 Michael Levin, and David A Relman. 2010. “Dissecting Interferon-Induced Transcriptional
997 Programs in Human Peripheral Blood Cells.” *PloS One* 5 (3): e9753.
998 doi:10.1371/journal.pone.0009753.
999 Walsh, Derek, Michael B Mathews, and Ian Mohr. 2013. “Tinkering with Translation: Protein
1000 Synthesis in Virus-Infected Cells.” *Cold Spring Harbor Perspectives in Biology* 5 (1):
1001 a012351. doi:10.1101/cshperspect.a012351.
1002 Wang, Jing, Dexter Duncan, Zhiao Shi, and Bing Zhang. 2013. “WEB-Based GEne SeT
1003 AnaLysis Toolkit (WebGestalt): Update 2013.” *Nucleic Acids Research* 41 (Web Server
1004 issue): W77–83. doi:10.1093/nar/gkt439.
1005 Wang, Liguo, Shengqin Wang, and Wei Li. 2012. “RSeQC: Quality Control of RNA-Seq
1006 Experiments.” *Bioinformatics (Oxford, England)* 28 (16): 2184–85.
1007 doi:10.1093/bioinformatics/bts356.
1008 Wichers, M C, G H Koek, G Robaeys, R Verkerk, S Scharpé, and M Maes. 2005. “IDO and
1009 Interferon-Alpha-Induced Depressive Symptoms: A Shift in Hypothesis from Tryptophan
1010 Depletion to Neurotoxicity.” *Molecular Psychiatry* 10 (6): 538–44.
1011 doi:10.1038/sj.mp.4001600.
1012 Wichers, Marieke C, and Michael Maes. 2004. “The Role of Indoleamine 2,3-Dioxygenase (IDO)
1013 in the Pathophysiology of Interferon-Alpha-Induced Depression.” *Journal of Psychiatry &*
1014 *Neuroscience : JPN* 29 (1): 11–17.
1015 Wiseman, Frances K., Tamara Al-Janabi, John Hardy, Annette Karmiloff-Smith, Dean Nizetic,
1016 Victor L. J. Tybulewicz, Elizabeth M. C. Fisher, and André Strydom. 2015. “A Genetic
1017 Cause of Alzheimer Disease: Mechanistic Insights from Down Syndrome.” *Nature Reviews*
1018 *Neuroscience* 16 (9). Nature Publishing Group, a division of Macmillan Publishers Limited.
1019 All Rights Reserved.: 564–74. doi:10.1038/nrn3983.
1020 Wörle, H, E Maass, B Köhler, and J Treuner. 1999. “Interferon Alpha-2a Therapy in
1021 Haemangiomas of Infancy: Spastic Diplegia as a Severe Complication.” *European Journal*

1022 *of Pediatrics* 158 (4): 344.

1023 Yao, Yihong, Brandon W Higgs, Laura Richman, Barbara White, and Bahija Jallal. 2010. "Use of
1024 Type I Interferon-Inducible mRNAs as Pharmacodynamic Markers and Potential Diagnostic
1025 Markers in Trials with Sifalimumab, an Anti-IFNα Antibody, in Systemic Lupus
1026 Erythematosus." *Arthritis Research & Therapy* 12 Suppl 1 (January): S6.
1027 doi:10.1186/ar2887.

1028 Zhang, Bing, Stefan Kirov, and Jay Snoddy. 2005. "WebGestalt: An Integrated System for
1029 Exploring Gene Sets in Various Biological Contexts." *Nucleic Acids Research* 33 (Web
1030 Server issue): W741–48. doi:10.1093/nar/gki475.

1031 Zitvogel, Laurence, Lorenzo Galluzzi, Oliver Kepp, Mark J Smyth, and Guido Kroemer. 2015.
1032 "Type I Interferons in Anticancer Immunity." *Nature Reviews. Immunology* 15 (7). Nature
1033 Publishing Group, a division of Macmillan Publishers Limited. All Rights Reserved.: 405–
1034 14. doi:10.1038/nri3845.

1035

1036 **FIGURE LEGENDS**

1037 **Figure 1. Transcriptome analysis identifies consistent changes in global gene expression**
1038 **between euploid (D21) and trisomy 21 (T21) fibroblasts.** (**A**) MA plots displaying the results
1039 of RNA-seq analysis for the indicated comparisons (see Figure 1- figure supplement 1A-C).
1040 Differentially expressed genes (DEGs), as defined by DEseq2 (FDR<10%), are labeled in red.
1041 (**B**) Volcano plots of comparisons in A highlight changes in chr21 gene expression (green)
1042 consistent with increased gene dosage effects. (**C**) Manhattan plots displaying DEGs (red) and
1043 all genes (black) for individual chromosomes do not show obvious domains of contiguous
1044 upregulation or down regulation. Shaded areas highlight regions of overlapping upregulation
1045 and downregulation (see Figure 1- figure supplements 2A and 3) (**D**) Violin plots of chr21 and
1046 non-chr21 DEGs displaying the distribution of fold changes of DEGs in each category. P-values
1047 were calculated with the Kolmogorov-Smirnov test. (**E**) Heatmap of all significant DEGs showing
1048 clustering of chr21 DEGs (green) around 1.5 fold upregulation in T21 cells. (**F**) Kernel density
1049 estimate plot highlighting the probabilities of chr21 DEGs (green, green dashed line indicates
1050 median), non-chr21 DEGs (black, black dashed line indicates median), and all genes (gray), of
1051 having a given fold change. (**G**) Box and whisker plot of standard deviations of fold changes in
1052 DEGs for six pairwise comparisons of age- and gender-matched T21 versus D21 fibroblasts
1053 showing greater variation in fold change for non-chr21 DEGs. P-values were calculated with the
1054 Kolmogorov-Smirnov test.

1055 **Figure 2. The interferon (IFN) transcriptional response is activated in trisomy 21 (T21)**
1056 **fibroblasts.** (**A**) Upstream regulator analysis of the T21-associated gene expression signature
1057 using Ingenuity Pathway Analysis (IPA) predicts numerous IFN-related factors as activated in
1058 T21 cells. (**B**) Representative results of the upstream regulator analysis for the Type I IFN ligand
1059 IFNA2. (**C**) Graphical summary of the observed deregulation of the IFN pathway in T21
1060 fibroblasts, showing the six IFN receptor subunits, four of which are encoded on chr21 and
1061 significantly upregulated in T21 fibroblasts; the predicted upstream regulators (orange),

1062 including the Type I, II, and III IFN ligands, as well as the IFN-activated transcription factors
1063 (IRFs and STATs); and select examples of Interferon Stimulated Genes (ISGs) upregulated in
1064 T21 fibroblasts, either encoded on chr21 (green) or elsewhere in the genome (gray). (**D**) Box
1065 and whisker plots showing RNA expression for the six IFN receptor subunits and select ISGs.
1066 chr21-encoded genes are highlighted in green. mRNA expression values are displayed in reads
1067 per kilobase per million (RPKM). Benjamini-Hochberg adjusted p-values were calculated using
1068 DESeq2. (**E**) Western blot analysis confirming upregulation of IFN receptors, STAT1
1069 phosphorylation, and ISGs, in T21 fibroblasts. (**F**) Box and whisker plots showing protein
1070 expression for select IFN-related genes as measured by SOMAscan assay. chr21-encoded
1071 genes are highlighted in green. Protein expression values are displayed in relative fluorescence
1072 units (RFU). Adjusted p-values were calculated using the Empirical Bayes method in QPROT.
1073 **Figure 3. T21 fibroblasts are more sensitive to IFN stimulation than D21 fibroblasts.** (**A**)
1074 Western blots showing that three T21 cell lines are more sensitive to IFNα treatment (24 hours)
1075 than age- and gender-matched D21 control cells as measured by induced expression of the
1076 ISGs MX1, IDO1 and ISG15. Elevated pSTAT1 levels confirm effective induction of the IFN
1077 pathway in response to ligand exposure. (**B**) Western blots as in **A** for IFN-β treatment. (**C**)
1078 Western blots as in **A** for IFN-γ treatment. * indicates non-specific bands.

1079 **Figure 4. An shRNA screen identifies the interferon (IFN)-activated kinases JAK1 and**
1080 **TYK2 as negative regulators of trisomy 21 (T21) cellular fitness.** (**A**) Schematic of kinome-
1081 focused shRNA screen to identify Differential Modulators of T21 (DM^{T21}) cellular fitness. (**B**)
1082 Volcano plot highlighting shRNAs targeting DM^{T21} genes that differentially inhibit T21 (blue) or
1083 euploid (D21, yellow) cellular fitness. Top hits were filtered by a FDR<5% and at least three
1084 shRNAs to the same gene scoring in one direction with no more than one shRNA scoring in the
1085 opposite direction. NRBP1 and JAK1 shRNAs are indicated with arrows. (**C**) Bar graphs of
1086 screen results for the IFN-related kinases JAK1 and TYK2, as well as mTOR, NRBP1, MAPK9

1087 and TSSK6. (**D**) Western blot analysis confirming downregulation of STAT1 phosphorylation
1088 and MX1 expression upon inhibition of JAK kinases with ruxolitinib (Rux) at the indicated
1089 concentrations in the GM2036-GM02767 cell pair. (**E**) Absolute cell numbers grown for 72 hours
1090 in their respective conditioned media with the indicated doses of Rux. (**F**) Relative cell numbers
1091 from (**E**). (**G**) Ratio of T21:D21 relative cell numbers demonstrates the overall differential effect
1092 of Rux on the number of viable cells from this T21-D21 pair. Results from a second cell line pair
1093 are shown in Figure 4 – figure supplement 1D-G. All data shown are an average of three
1094 experiments ± standard error of the mean.

1095 **Figure 5. Activation of the interferon (IFN) transcriptional response is conserved in**
1096 **trisomy 21 (T21) lymphoblastoid cell lines**. (**A**) MA plot displaying the gene expression
1097 signature associated with T21 in a panel of six lymphoblastoid cell lines, three of which harbor
1098 T21. Differential expressed genes (DEGs), as defined by DEseq2 (FDR<10%), are labeled in
1099 red. (**B**) Volcano plot of DEGs with those encoded on chr21 highlighted in green. (**C**) Manhattan
1100 plot of chr21 with DEGs in red and all other genes in black. (**D**) Upstream regulator analysis
1101 reveals activation of the IFN transcriptional response in T21 lymphoblastoid cell lines. (**E**)
1102 Comparative analysis between fibroblasts and lymphoblastoids highlights conserved upstream
1103 regulators within the IFN pathway. (**F**) Box and whisker plots of RNA expression for the four IFN
1104 receptor subunits encoded on chr21 (green) and three interferon-related genes (black). mRNA
1105 expression values are displayed in reads per kilobase per million (RPKM). Benjamini-Hochberg
1106 adjusted p-values were calculated using DESeq2. (**G**) Western blot analysis confirming
1107 upregulation of IFN receptors, pSTAT1, and interferon related genes, at the protein level in T21
1108 lymphoblastoids.

1109 **Figure 6. IFN signaling is activated in circulating blood cells from individuals with T21.**
1110 (**A**) Box and whisker plots of RNA expression for the four IFN receptor subunits encoded on
1111 chr21 and representative IFN-related genes in circulating monocytes. mRNA expression values
1112 are displayed in reads per kilobase per million (RPKM). Benjamini-Hochberg adjusted p-values

1113 were calculated using DESeq2. (**B**) Box and whisker plots of RNA expression as in (A) for
1114 circulating T cells. (**C**) Upstream regulator analysis reveals activation of the IFN transcriptional
1115 response in T21 monocytes and T cells, as well as downregulation of the MYCN-driven
1116 transcriptional program. (**D**) Canonical pathway analysis reveals activation of the IFN signaling
1117 pathway in T21 monocytes and T cells, as well as downregulation of the EIF2 signaling
1118 pathway.

1119 **Figure 7. Trisomy 21 globally downregulates the translational machinery in monocytes**
1120 **and T cells.** (**A**) Venn diagram demonstrating the overlap in DEGs comprising the MYCN
1121 upstream regulator and EIF2 signaling pathway gene signatures identified by IPA in monocytes.
1122 Prominent components of each group are indicated with arrows. See also Figure 7 – figure
1123 supplements 2 and 3. (**B**) Box and whisker plots of RNA expression for representative
1124 translation-related genes from monocytes. mRNA expression values are displayed in reads per
1125 kilobase per million (RPKM). Benjamini-Hochberg adjusted p-values were calculated using
1126 DESeq2. (**C**) Venn diagram demonstrating the overlap in DEGs as in (A) for T cells. (**D**) Box and
1127 whisker plots of RNA expression as in (C) for T cells.

1128 **Figure 8. Trisomy 21 activates the IFN gene expression program in a cell type-specific**
1129 **manner.** (**A**) Principal component analysis (PCA) of all RNA-seq samples from this study
1130 colored by cell type. (**B**) PCA analysis as in (A) colored by chr21 copy number. (**C**) Box and
1131 whisker plots of RNA expression for representative chr21-encoded genes from all samples.
1132 mRNA expression values are displayed in reads per kilobase per million (RPKM). Benjamini-
1133 Hochberg adjusted p-values were calculated using DESeq2 by comparing all T21 samples to all
1134 D21 samples. Individual data points are colored by cell type. (**D**,**E**) Box and whisker plots as in
1135 (C) for chr21-encoded IFN receptors and representative ISGs. (**F**) Venn diagram showing the
1136 cell type-specificity of the *Interferon alpha* gene expression programs identified by IPA for each
1137 cell type. (**G**) Manhattan plots for chromosomes 19 and 21 comparing the DEGs from
1138 monocytes and T cells derived from the same individuals.

1139 **Figure 1 – figure supplement 1. T21 and D21 fibroblast RNA-seq.** (**A**) Description of
1140 fibroblast cell lines used in this study. (**B**) Principal component analysis (PCA) of fibroblast RNA-
1141 seq samples demonstrates tight grouping of biological replicates. (**C**) Schematic of group
1142 comparisons. (**D**) PCR of genomic DNA for the *RCAN1* gene encoded on chr21 confirms T21
1143 status. *RPLP0* is a control gene encoded on chr12. (**E**) Bar graph displaying how numbers of
1144 differentially expressed genes (DEGs) encoded on chr21 increase with sample size.
1145 **Figure 1 – figure supplement 2. Amplification of changes in gene expression emanating**
1146 **from T21.** (**A**) Manhattan plot showing most DEGs (red) are not encoded on chr21. (**B**)
1147 Example box and whisker plots of chr21 (green) and non-chr21 (black) DEGs. mRNA
1148 expression values are displayed in reads per kilobase per million (RPKM). Benjamini-Hochberg
1149 adjusted p-values were calculated using DESeq2.
1150 **Figure 1 – figure supplement 3**. **Differentially expressed genes in trisomy 21 fibroblasts**
1151 **are not organized into obvious chromatin domains.** Manhattan plots for individual
1152 chromosomes indicating differentially expressed genes in red.
1153 **Figure 2 – figure supplement 1. Network analysis confirms IFN activation signature in T21**
1154 **cells.** (**A**) IPA upstream regulator analysis of genes activated upon MDM2 inhibition with Nutlin-
1155 3, hypoxia (1% O_2), and serum stimulation in HCT116 colorectal cancer cells correctly identifies
1156 the transcription factor p53, the transcription factor HIF1A, and the growth factor PDGF, as the
1157 key upstream regulators in each scenario. (**B**) Top 15 deregulated pathways in T21 cells
1158 identified by Pathway Commons Analysis in WebGestalt. IFN-related pathways are highlighted
1159 in red. (**C**) Pie charts showing the percentage of chr21 and non-chr21 upregulated genes in the
1160 interferon pathway.
1161 **Figure 4 – figure supplement 1. An shRNA screen identifies Differential Modulators of**
1162 **T21 (DM^{T21}) cellular fitness.** (**A, B**) shRNAs targeting DM^{T21} genes that differentially inhibit T21
1163 (blue) or D21 (yellow) cellular fitness. (**C**) Q-RT-PCR demonstrating that Ruxolitinib (Rux)
1164 treatment downregulates mRNA expression for many ISGs in a dose-dependent manner. (**D**)

1165 Western blots demonstrating effect of Rux treatment on pSTAT1 and MX1 on the cell line pair
1166 GM05659 (D21) and AG05397 (T21) (pair 2). (**E**) Absolute cell numbers from pair 2 grown for
1167 72 hours in their respective conditioned media with the indicated doses of Rux. (**F**) Relative cell
1168 numbers from (**E**). (**G**) Ratio of T21:D21 relative cell numbers demonstrates the overall
1169 differential effect of Rux on the number of viable cells from this T21-D21 pair. All data shown are
1170 an average of three experiments ± standard error of the mean.

1171 **Figure 5 – figure supplement 1. Biological replicates of lymphoblastoid samples are**
1172 **highly related.** (**A**) Table of lymphoblastoid cell lines used in this study. All lymphoblastoid lines
1173 used are female. (**B**) Principal component analysis (PCA) of RNA-seq samples from
1174 lymphoblastoid cell lines.

1175 **Figure 5 – figure supplement 2. Differentially expressed genes in trisomy 21**
1176 **lymphoblastoid cell lines are not organized into obvious chromatin domains.** Manhattan
1177 plots for individual chromosomes indicating differentially expressed genes in red.

1178 **Figure 5 – figure supplement 3. Components of the IFN response are activated in a**
1179 **mouse model of Down syndrome.** (**A**) Principal component analysis (PCA) of RNA-seq
1180 samples produced from lineage negative, Sca1 positive, c-kit positive (LSK) cells from Dp16
1181 mice and matched littermate controls. (**B**) Box and whisker plots of RNA expression for the four
1182 IFN receptor subunits encoded on chr16 (green) and representative IFN-related genes from
1183 Dp16 LSK cells. mRNA expression values are displayed in reads per kilobase per million
1184 (RPKM). Benjamini-Hochberg adjusted p-values were calculated using DESeq2.

1185 **Figure 6 – figure supplement 1. Effects of T21 on the transcriptome of circulating**
1186 **monocytes and T cells from individuals with T21 and typical controls.** (**A**) Description of
1187 samples from individuals with T21 and typical controls used in this study. (**B**) Principal
1188 component analysis (PCA) of monocyte and T cell RNA-seq samples. (**C**) MA plots displaying
1189 the results of RNA-seq analysis for monocytes and T cells. Differentially expressed genes
1190 (DEGs), as defined by DEseq2 (FDR<10%), are labeled in red. (**D**) Volcano plots of data from

1191 monocytes and T cells highlight changes in chr21 gene expression (green) consistent with
1192 increased gene dosage effects.
1193 **Figure 6 – figure supplement 2. Surface expression of IFN receptors is increased in B**
1194 **cells from individuals with T21.** Flow cytometric analysis of surface expression of three chr21-
1195 encoded IFN receptors (in green) and one encoded on another chromosome (IFNGR1) in B
1196 cells isolated from the same individuals as monocytes and T cells used in Figure 6.
1197 **Figure 6 – figure supplement 3. The IFN gene signature from monocytes and T cells is**
1198 **largely encoded by non-chr21 genes.** IPA upstream regulator analysis of all DEGs, non-chr21
1199 DEGs, and chr21 DEGs, for monocytes and T cells.
1200 **Figure 7 – figure supplement 1. The MYCN transcriptional program is downregulated by**
1201 **T21.** A heatmap demonstrates downregulation of numerous components of the translational
1202 machinery associated with MYCN-driven transcription in monocytes from individuals with T21.
1203 Data presented are the fold change of the RPKM of each sample relative to the mean RPKM of
1204 all D21 individuals.
1205 **Figure 7 – figure supplement 2. The EIF2 Signaling pathway is downregulated by T21.** A
1206 heatmap demonstrates downregulation of numerous components of the translational machinery
1207 associated with EIF2 Signaling in monocytes from individuals with T21. Data presented are the
1208 fold change of the RPKM of each sample relative to the mean RPKM of all D21 individuals.
1209 **Supplementary file 1. (A) Fibroblast, (B) lymphoblastoid, (C) Dp16, (D) monocyte, (E) T**
1210 **cell and (F) meta RNA-seq.** DESeq2 analysis of T21 versus D21 fibroblasts. Columns include:
1211 (A) Chromosome, (B) Gene start coordinate, (C) Gene end coordinate, (D) Gene strand, (E)
1212 Gene name, (F) basemean (average read count across all samples), (G) basemeanD21
1213 (average read count across all D21 samples), (H) basemeanT21 (average read count across all
1214 T21 samples), (I) foldChange (basemeanT21/basemeanD21), (J) log2FoldChange, (K)
1215 foldChange_adj (DESeq2 adjusted fold change), (L) log2FoldChange_adj, (M) pval (p-value),
1216 (N) padj (Benjamini-Hochberg adjusted p-value).

1217 **Supplementary file 2. Fibroblast kinome shRNA screen analysis.** DESeq2 analysis of
1218 kinome shRNA screens in T21 versus D21 fibroblasts. Columns include: (A) TRC number (B)
1219 shRNA targeting location (C) Chromosome, (D) Genomic coordinates, (E) Gene strand, (F)
1220 Gene name, (G) RefSeq ID (H) basemean (average read count across all samples), (I)
1221 basemeanD21 (average read count across all D21 samples), (J) basemeanT21 (average read
1222 count across all T21 samples), (K) foldChange (basemeanT21/basemeanD21), (L)
1223 log2FoldChange, (M) foldChange_adj (DESeq2 adjusted fold change), (N)
1224 log2FoldChange_adj, (O) pval (p-value), (P) padj (Benjamini-Hochberg adjusted p-value).
1225 **Supplementary file 3. Fibroblast SOMAscan analysis.** QPROT analysis of T21 versus D21
1226 fibroblasts. Columns include: (A) Chromosome, (B) Gene start coordinate, (C) Gene end
1227 coordinate, (D) Gene strand, (E) Gene name, (F) RFUmean (average RFU across all samples),
1228 (G) RFUmeanD21 (average RFU across all D21 samples), (H) RFUmeanT21 (average RFU
1229 across all T21samples), (I) foldChange (RFUmeanT21/RFUmeanD21), (J) log2FoldChange, (K)
1230 Zstatistic (Z-score from QPROT), (L) FDRup (FDR of upregulated proteins), (M) FDRdown
1231 (FDR of downregulated proteins).
1232

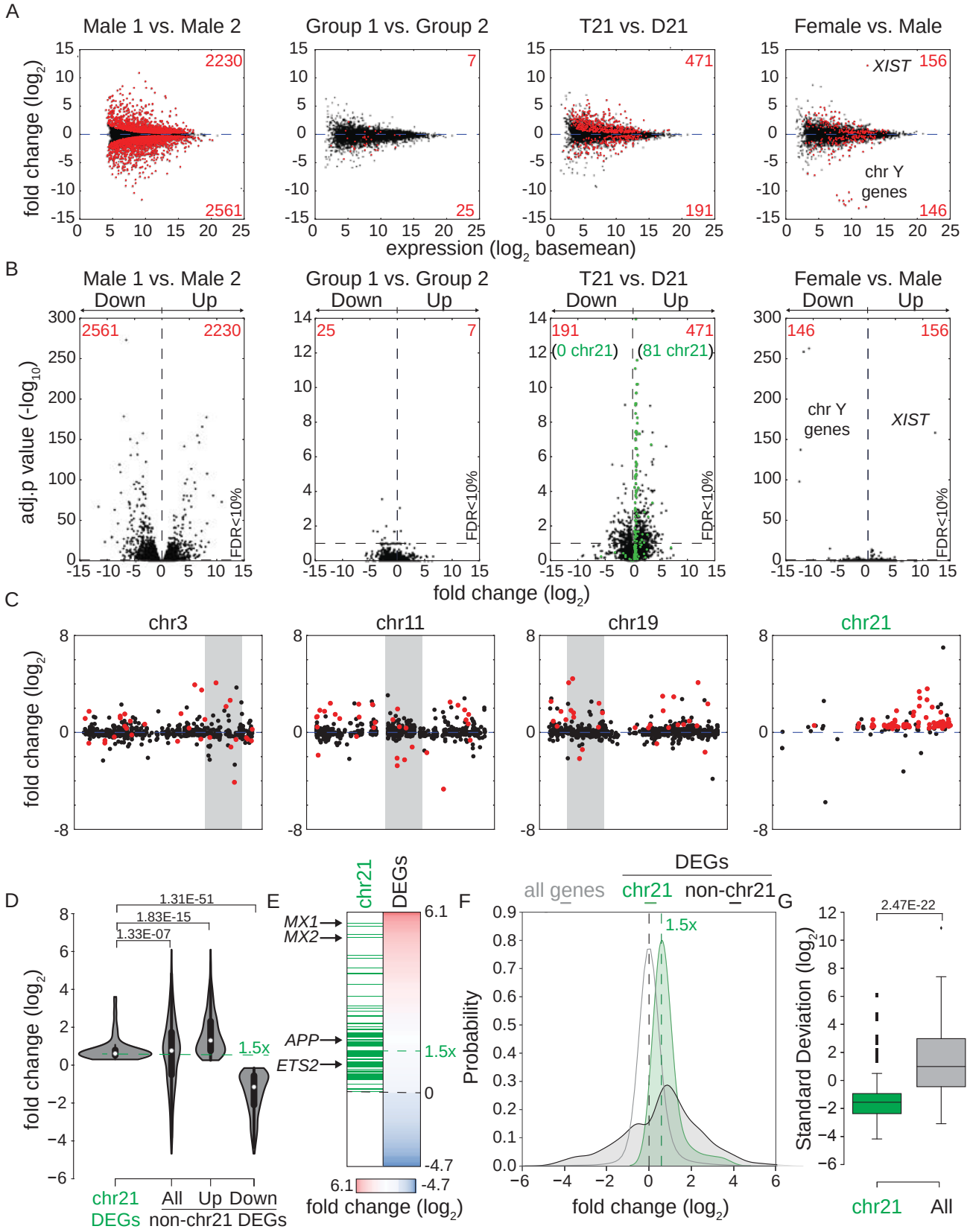

Figure 1. Transcriptome analysis identifies consistent changes in global gene expression between euploid (D21) and trisomy 21 (T21) fibroblasts. (**A**) MA plots displaying the results of RNA-seq analysis for the indicated comparisons (see Figure 1- figure supplement 1A-C). Differentially expressed genes (DEGs), as defined by DEseq2 (FDR<10%), are labeled in red. (**B**) Volcano plots of comparisons in A highlight changes in chr21 gene expression (green) consistent with increased gene dosage effects. (**C**) Manhattan plots displaying DEGs (red) and all genes (black) for individual chromosomes do not show obvious domains of contiguous upregulation or down regulation. Shaded areas highlight regions of overlapping upregulation and downregulation (see Figure 1- figure supplements 2A and 3) (**D**) Violin plots of chr21 and non-chr21 DEGs displaying the distribution of fold changes of DEGs in each category. P-values were calculated with the Kolmogorov-Smirnov test. (**E**) Heatmap of all significant DEGs showing clustering of chr21 DEGs (green) around 1.5 fold upregulation in T21 cells. (**F**) Kernel density estimate plot highlighting the probabilities of chr21 DEGs (green, green dashed line indicates median), non-chr21 DEGs (black, black dashed line indicates median), and all genes (gray), of having a given fold change. (**G**) Box and whisker plot of standard deviations of fold changes in DEGs for six pairwise comparisons of age- and gender-matched T21 versus D21 fibroblasts showing greater variation in fold change for non-chr21 DEGs. P-values were calculated with the Kolmogorov-Smirnov test.

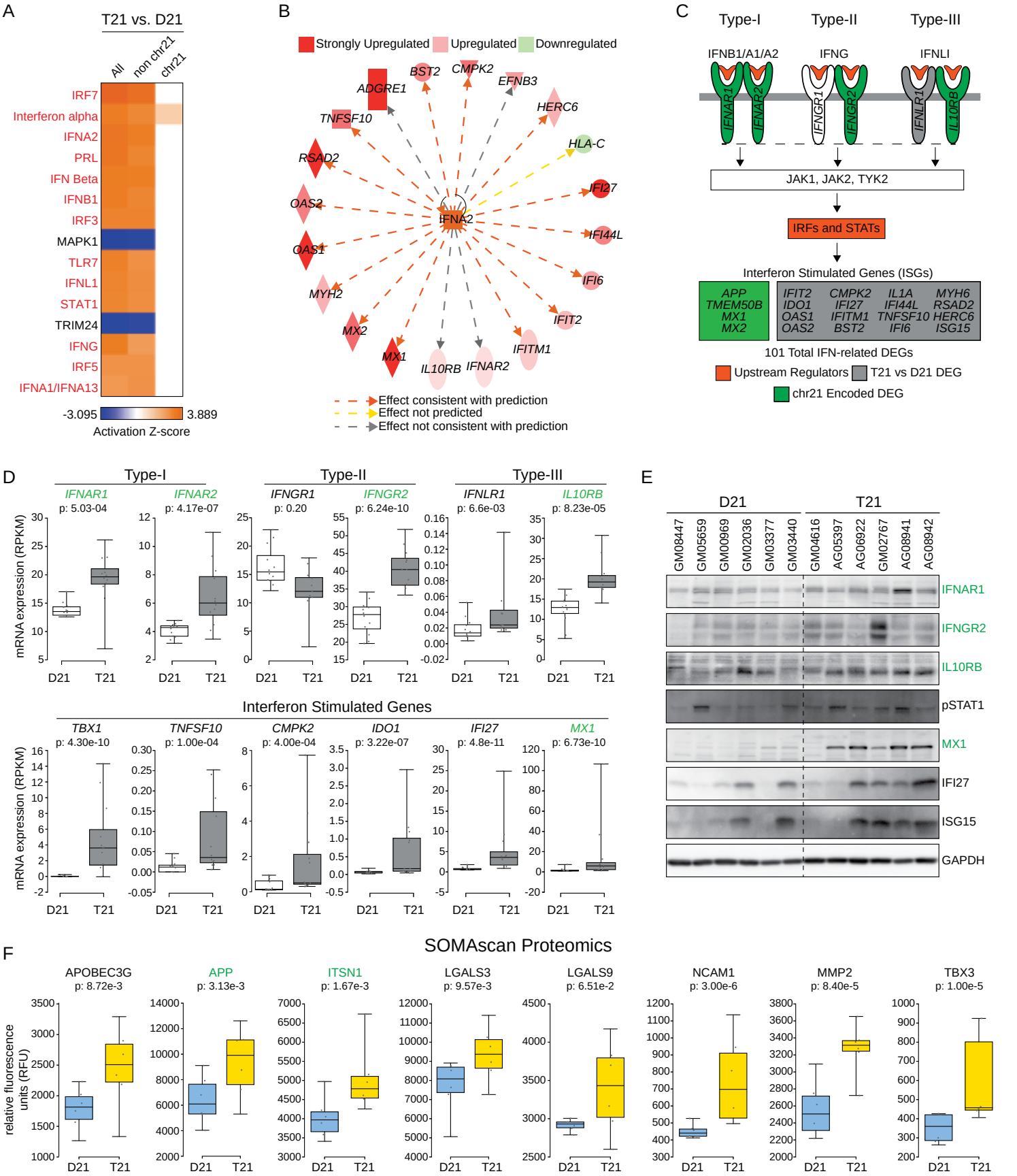

Figure 2. The interferon (IFN) transcriptional response is activated in trisomy 21 (T21) fibroblasts. (**A**) Upstream regulator analysis of the T21-associated gene expression signature using Ingenuity Pathway Analysis (IPA) predicts numerous IFN-related factors as activated in T21 cells. (**B**) Representative results of the upstream regulator analysis for the Type I IFN ligand IFNA2. (**C**) Graphical summary of the observed deregulation of the IFN pathway in T21 fibroblasts, showing the six IFN receptor subunits, four of which are encoded on chr21 and significantly upregulated in T21 fibroblasts; the predicted upstream regulators (orange), including the Type I, II, and III IFN ligands, as well as the IFN-activated transcription factors (IRFs and STATs); and select examples of Interferon Stimulated Genes (ISGs) upregulated in T21 fibroblasts, either encoded on chr21 (green) or elsewhere in the genome (gray). (**D**) Box and whisker plots showing RNA expression for the six IFN receptor subunits and select ISGs. chr21-encoded genes are highlighted in green. mRNA expression values are displayed in reads per kilobase per million (RPKM). Benjamini-Hochberg adjusted p-values were calculated using DESeq2. (**E**) Western blot analysis confirming upregulation of IFN receptors, STAT1 phosphorylation, and ISGs, in T21 fibroblasts. (**F**) Box and whisker plots showing protein expression for select IFN-related genes as measured by SOMAscan assay. chr21-encoded genes are highlighted in green. Protein expression values are displayed in relative fluorescence units (RFU). Adjusted p-values were calculated using the Empirical Bayes method in QPROT.

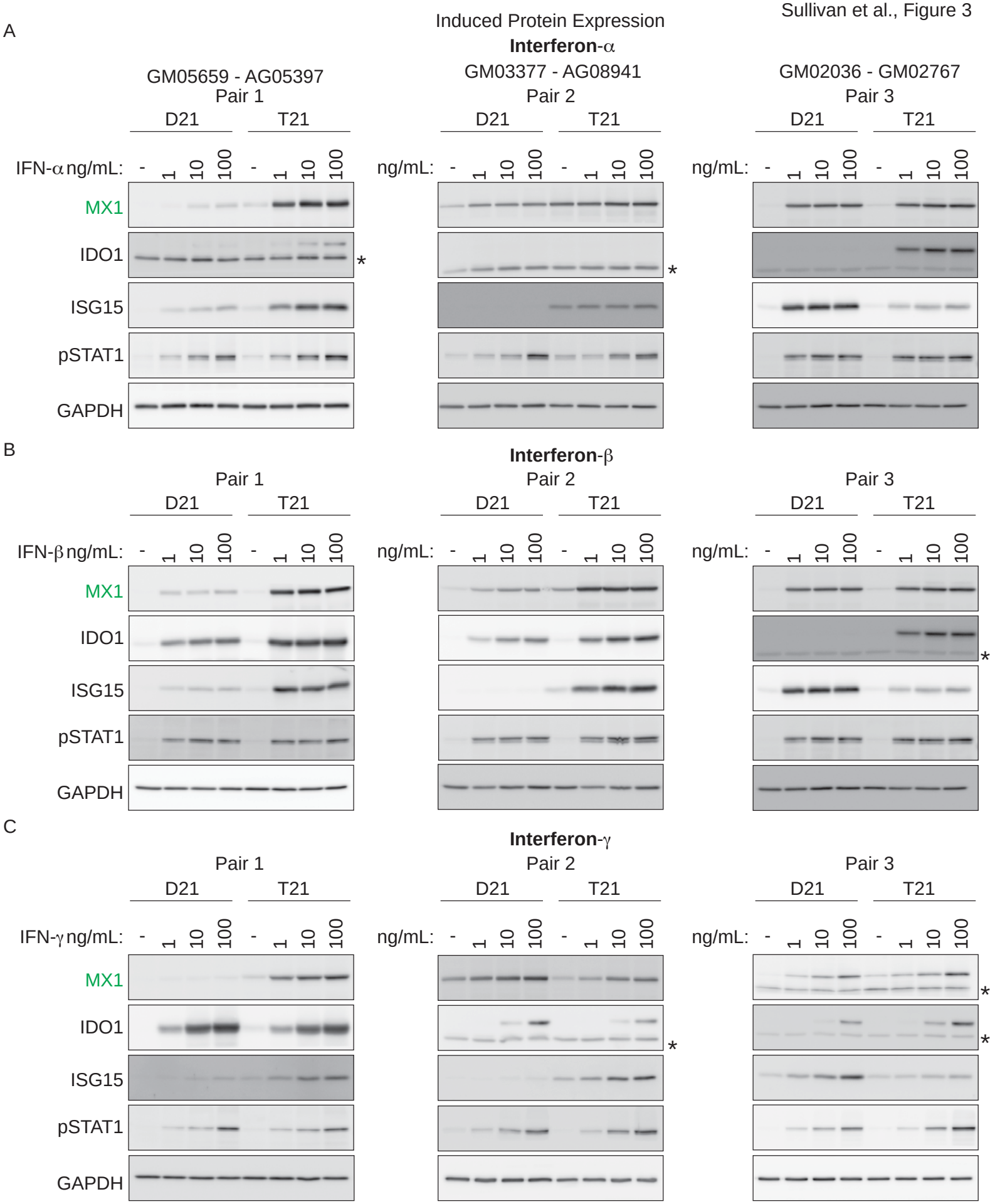

Figure 3. T21 fibroblasts are more sensitive to IFN stimulation than D21 fibroblasts. (**A**) Western blots showing that three T21 cell lines are more sensitive to IFN-α treatment (24 hours) than age- and gender-matched D21 control cells as measured by induced expression of the ISGs MX1, IDO1 and ISG15. Elevated pSTAT1 levels confirm effective induction of the IFN pathway in response to ligand exposure. (**B**) Western blots as in A for IFN-β treatment. (**C**) Western blots as in A for IFN-γ treatment. * indicates non-specific bands.

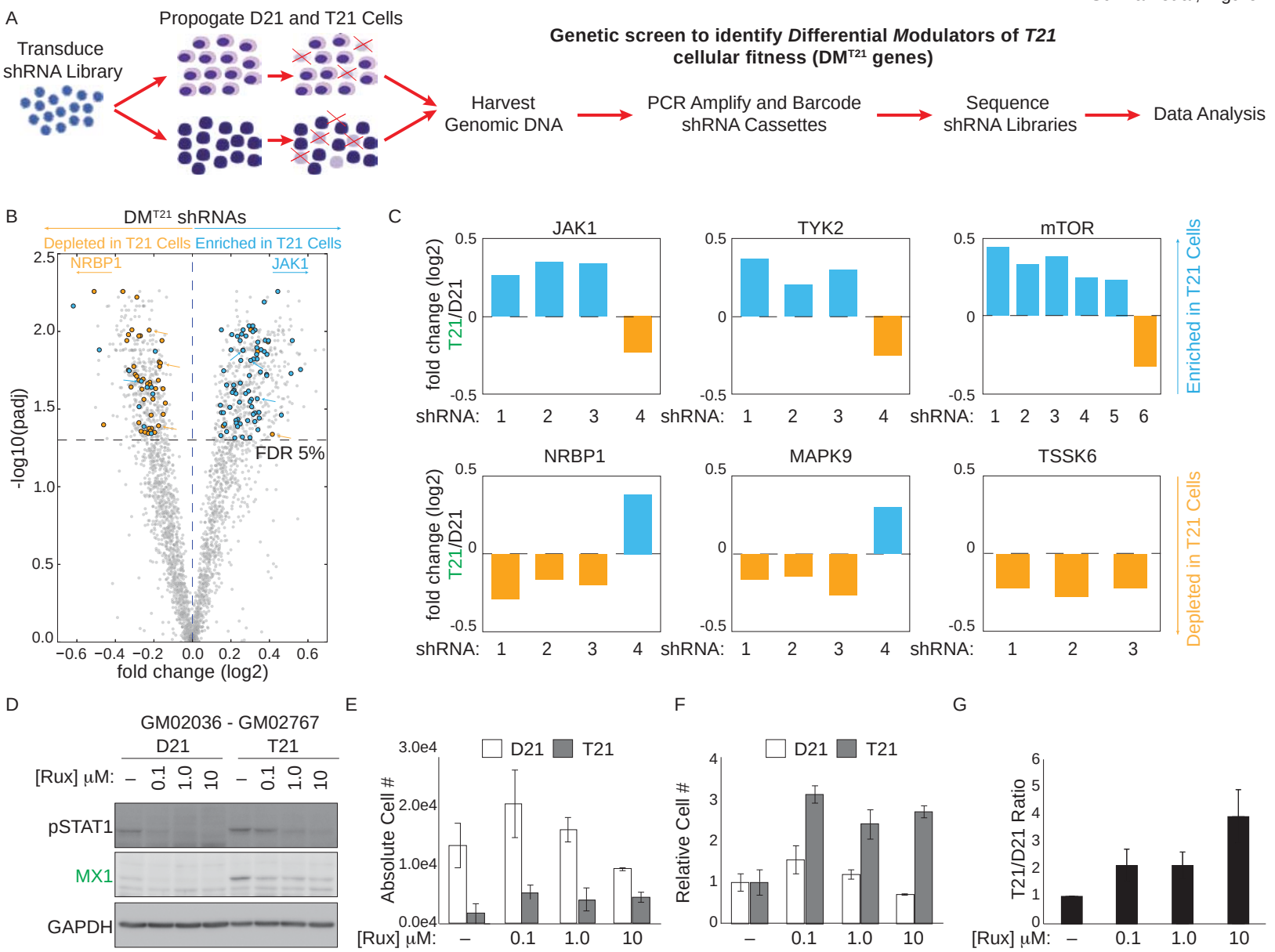

Figure 4. An shRNA screen identifies the interferon (IFN)-activated kinases JAK1 and TYK2 as negative regulators of trisomy 21 (T21) cellular fitness. (**A**) Schematic of kinome-focused shRNA screen to identify Differential Modulators of T21 (DM^{T21}) cellular fitness. (**B**) Volcano plot highlighting shRNAs targeting DM^{T21} genes that differentially inhibit T21 (blue) or euploid (D21, yellow) cellular fitness. Top hits were filtered by a FDR<5% and at least three shRNAs to the same gene scoring in one direction with no more than one shRNA scoring in the opposite direction. NRBP1 and JAK1 shRNAs are indicated with arrows. (**C**) Bar graphs of screen results for the IFN-related kinases JAK1 and TYK2, as well as mTOR, NRBP1, MAPK9 and TSSK6. (**D**) Western blot analysis confirming downregulation of STAT1 phosphorylation and MX1 expression upon inhibition of JAK kinases with ruxolitinib (Rux) at the indicated concentrations in the GM2036-GM02767 cell pair. (**E**) Absolute cell numbers grown for 72 hours in their respective conditioned media with the indicated doses of Rux. (**F**) Relative cell numbers from (E). (**G**) Ratio of T21:D21 relative cell numbers demonstrates the overall differential effect of Rux on the number of viable cells from this T21-D21 pair. Results from a second cell line pair are shown in Figure 4 – figure supplement 1D-G. All data shown are an average of three experiments ± standard error of the mean.

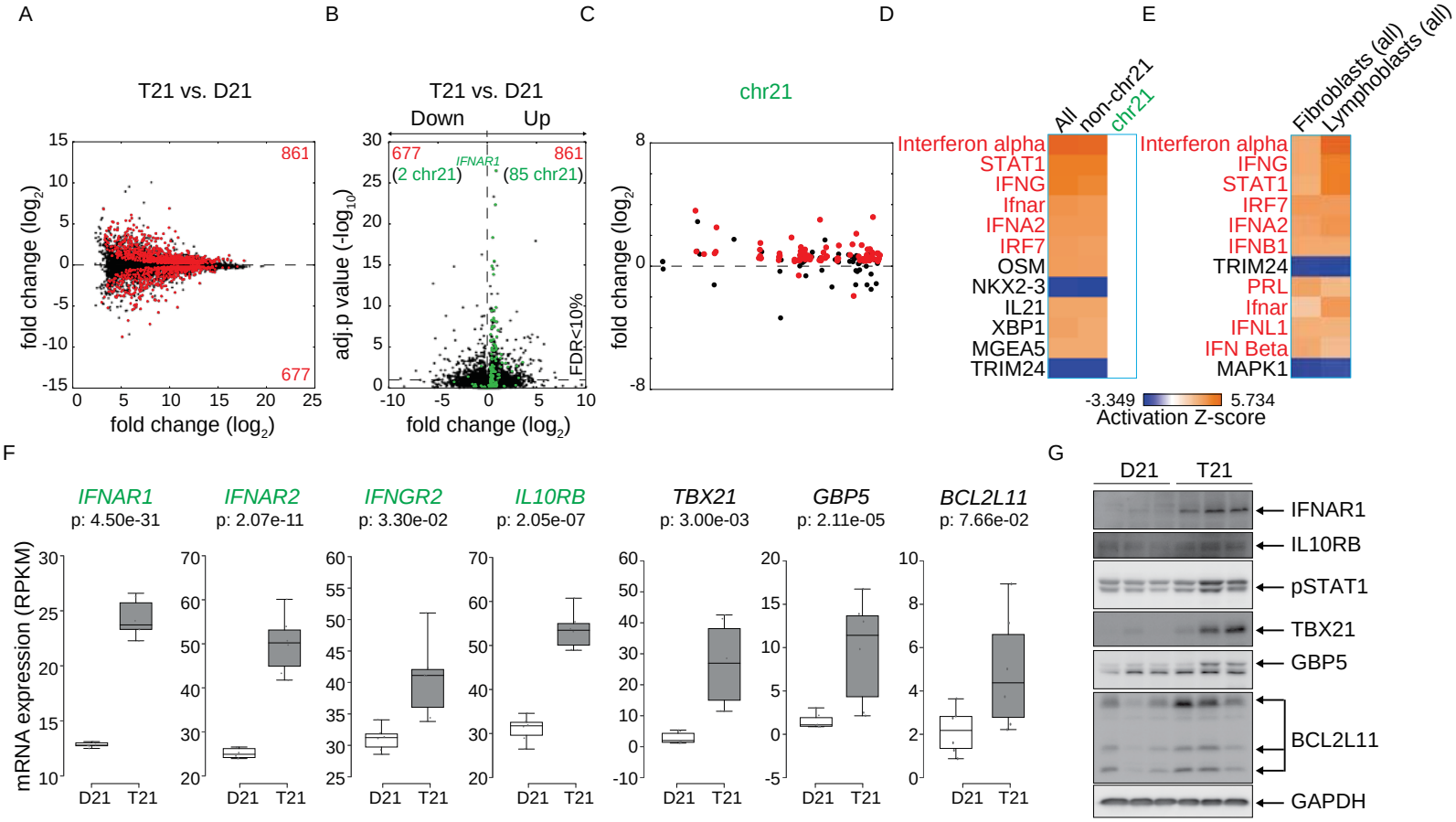

Figure 5. Activation of the interferon (IFN) transcriptional response is conserved in trisomy 21 (T21) lymphoblastoid cell lines. (**A**) MA plot displaying the gene expression signature associated with T21 in a panel of six lymphoblastoid cell lines, three of which harbor T21. Differential expressed genes (DEGs), as defined by DEseq2 (FDR<10%), are labeled in red. (**B**) Volcano plot of DEGs with those encoded on chr21 highlighted in green. (**C**) Manhattan plot of chr21 with DEGs in red and all other genes in black. (**D**) Upstream regulator analysis reveals activation of the IFN transcriptional response in T21 lymphoblastoid cell lines. (**E**) Comparative analysis between fibroblasts and lymphoblastoids highlights conserved upstream regulators within the IFN pathway. (**F**) Box and whisker plots of RNA expression for the four IFN receptor subunits encoded on chr21 (green) and three interferon-related genes (black). mRNA expression values are displayed in reads per kilobase per million (RPKM). Benjamini-Hochberg adjusted p-values were calculated using DESeq2. (**G**) Western blot analysis confirming upregulation of IFN receptors, pSTAT1, and interferon related genes, at the protein level in T21 lymphoblastoids.

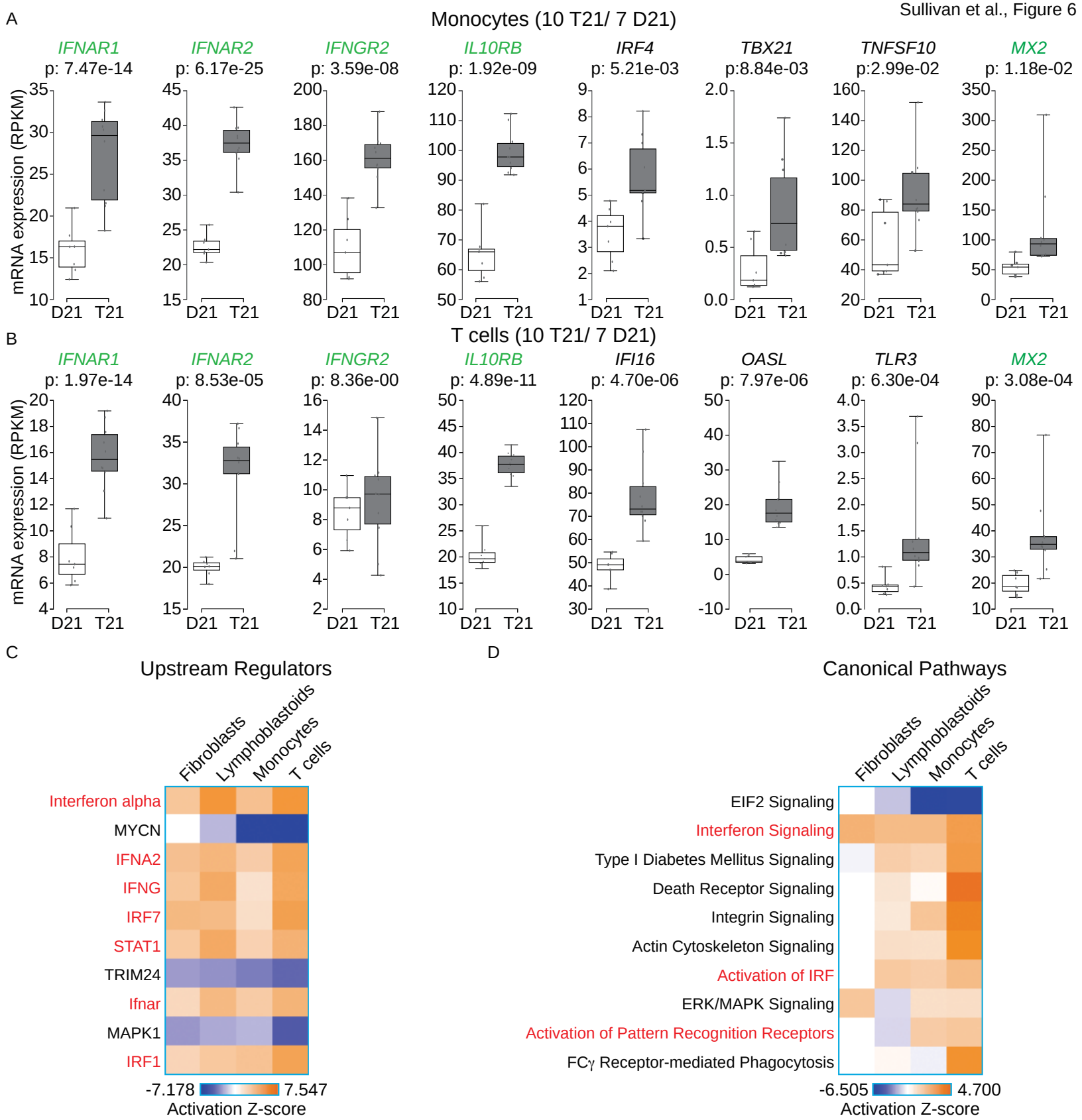

Figure 6. IFN signaling is activated in circulating blood cells from individuals with T21. (**A**) Box and whisker plots of RNA expression for the four IFN receptor subunits encoded on chr21 and representative IFN-related genes in circulating monocytes. mRNA expression values are displayed in reads per kilobase per million (RPKM). Benjamini-Hochberg adjusted p-values were calculated using DESeq2. (**B**) Box and whisker plots of RNA expression as in (A) for circulating T cells. (**C**) Upstream regulator analysis reveals activation of the IFN transcriptional response in T21 monocytes and T cells, as well as downregulation of the MYCN-driven transcriptional program. (**D**) Canonical pathway analysis reveals activation of the IFN signaling pathway in T21 monocytes and T cells, as well as downregulation of the EIF2 signaling pathway.

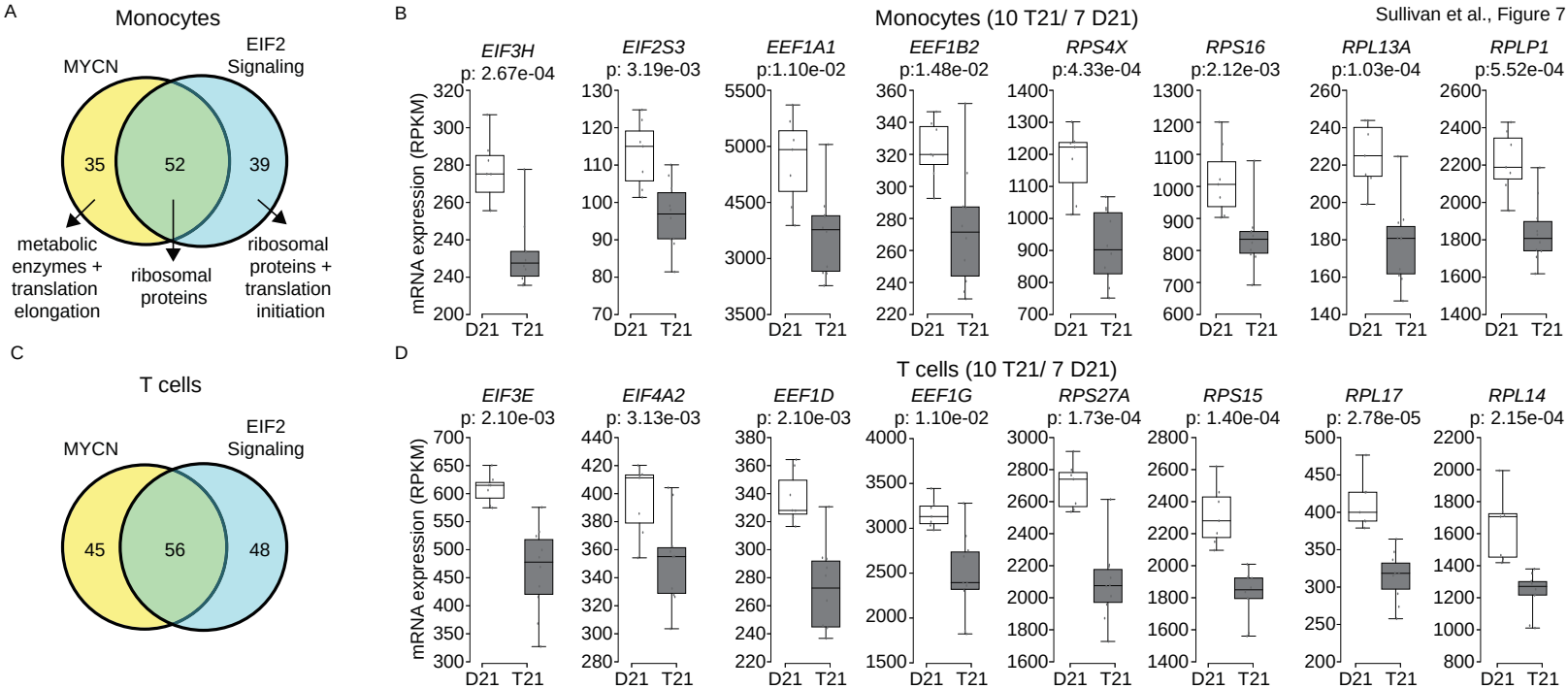

Figure 7. Trisomy 21 globally downregulates the translational machinery in monocytes and T cells. (**A**) Venn diagram demonstrating the overlap in DEGs comprising the MYCN upstream regulator and EIF2 signaling pathway gene signatures identified by IPA in monocytes. Prominent components of each group are indicated with arrows. See also Figure 7 – figure supplements 2 and 3. (**B**) Box and whisker plots of RNA expression for representative translation-related genes from monocytes. mRNA expression values are displayed in reads per kilobase per million (RPKM). Benjamini-Hochberg adjusted p-values were calculated using DESeq2. (**C**) Venn diagram demonstrating the overlap in DEGs as in (A) for T cells. (**D**) Box and whisker plots of RNA expression as in (C) for T cells.

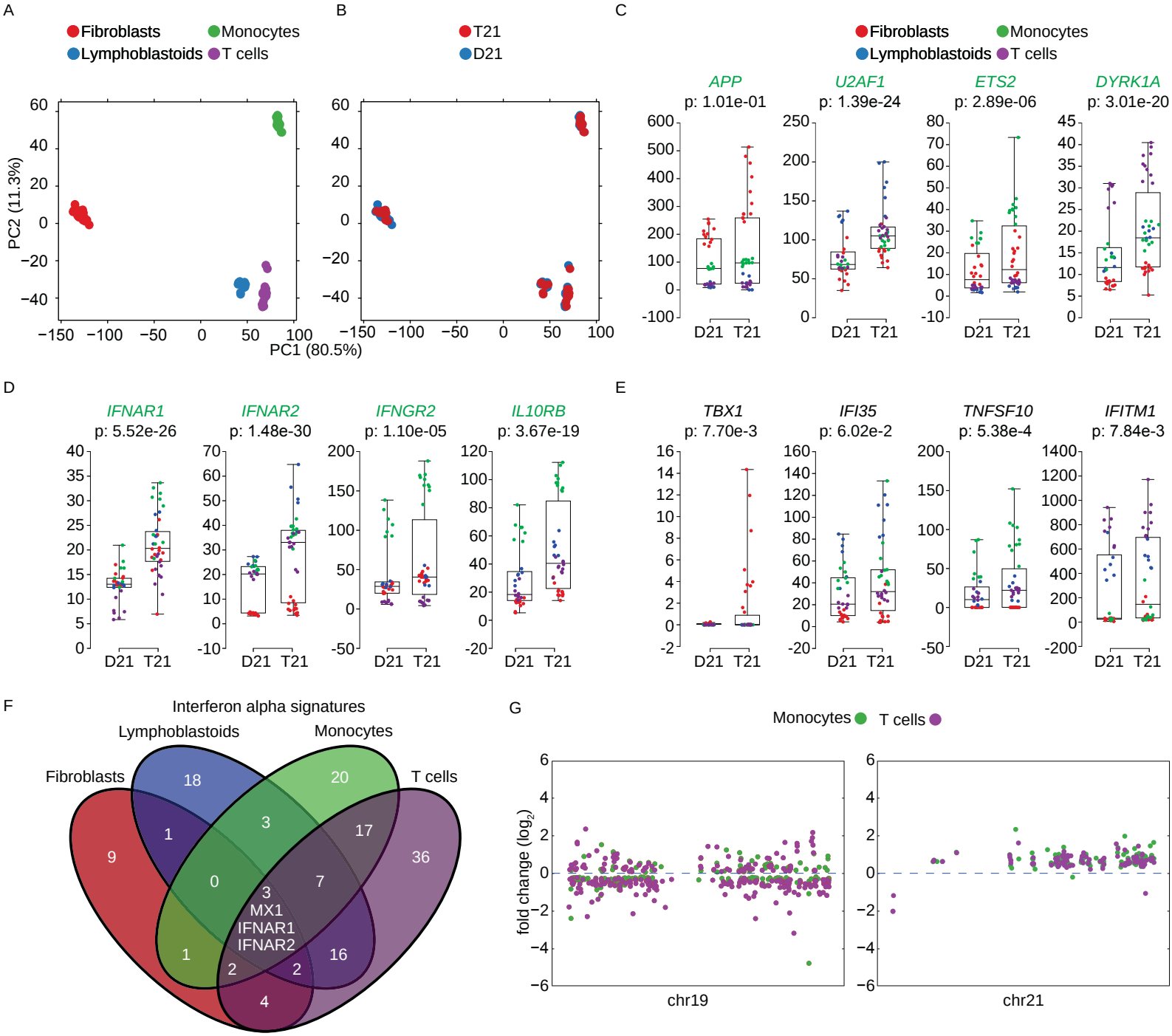

Figure 8. Trisomy 21 activates the IFN gene expression program in a cell type-specific manner. (**A**) Principal component analysis (PCA) of all RNA-seq samples from this study colored by cell type. (**B**) PCA analysis as in (A) colored by chr21 copy number. (**C**) Box and whisker plots of RNA expression for representative chr21-encoded genes from all samples. mRNA expression values are displayed in reads per kilobase per million (RPKM). Benjamini-Hochberg adjusted p-values were calculated using DESeq2 by comparing all T21 samples to all D21 samples. Individual data points are colored by cell type. (**D**,**E**) Box and whisker plots as in (C) for chr21-encoded IFN receptors and representative ISGs. (**F**) Venn diagram showing the cell type-specificity of the Interferon alpha gene expression programs identified by IPA for each cell type. (**G**) Manhattan plots for chromosomes 19 and 21 comparing the DEGs from monocytes and T cells derived from the same individuals.